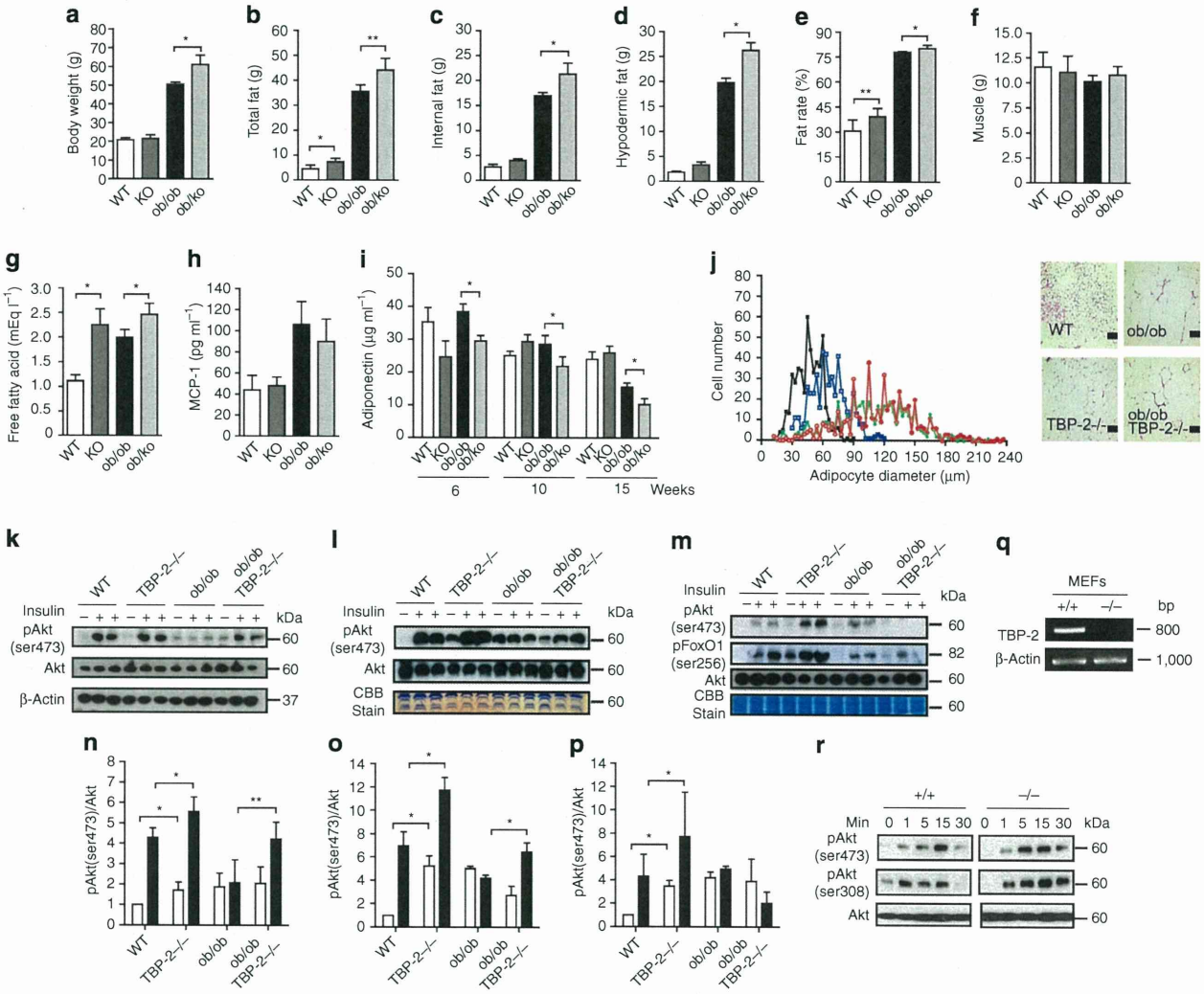

Figure 2 | TBP-2 deficiency ameliorates insulin resistance and increase Akt signalling. (**a**–**f**) Fat and muscle content. Body weight (**a**), total fat (**b**), internal fat (**c**), hypodermic fat (**d**), fat rate (**e**), muscle (**f**) in male WT (WT), TBP-2−/− (KO), ob/ob (ob/ob) and ob/ob·TBP-2−/− (ob/ko) mice calculated from computed tomography scan data are shown for 15 weeks aged mice, $N \geq 4$. (**g**, **h**) Serum physiological parameters. Free fatty acid (**g**) and MCP-1 (**h**) were measured in 15 weeks aged mice, $N \geq 7$. (**i**) Blood adiponectin concentration was measured in 6, 10 and 15 weeks aged mice, $n = \geq 5$. (**j**) Distribution of adipocyte size in white adipose from 10 weeks aged WT (black closed rectangle), TBP-2−/− (blue open rectangle), ob/ob (green closed circle) and ob/ob·TBP-2−/− (red open circle) mice (left panel). The right panel shows histological analyses of haematoxylin and eosin (HE)-stained white adipose sections in these mice. Scale bar indicates 100 μm. (**k**–**m**) Immuno blotting (IB) analyses of ser473-phospholylated Akt (pAkt), ser256-phospholylated FoxO1 (pFoxO1) and total Akt in response to insulin (2 U kg^{-1}) in skeletal muscle (**k**), heart (**l**) and liver (**m**). Densitometric quantification of pAkt/Akt ratios in skeletal muscle (**n**), heart (**o**) and liver (**p**). Open and closed bar represents without or with insulin stimulation, respectively. (**q**) Loss of endogenous TBP-2 mRNA in MEFs. (**r**) IB analyses. TBP-2 deficiency enhances insulin/Akt signalling in primary MEFs. MEFs were serum starved for 12 h and then stimulated with insulin (100 nM) for different times. Data are presented as mean±s.d. *P< 0.05, **P< 0.01, versus control (t-test).

(Fig. 4l). These results showed that mitochondrial morphological changes and metabolic dysfunctions in β-cells are improved by TBP-2 deficiency in ob/ob mice.

TBP-2 suppresses mitochondrial ATP production and GSIS. To delineate how TBP-2 deficiency protects against the impaired GSIS in ob/ob islets, we next examined the dose effect of TBP-2 on GSIS in the rat β-cell line INS-1 cells. Silencing of TBP-2 (RNAi1 and RNAi2) enhanced GSIS in INS-1 cells (Fig. 5a,b,d). On the contrary, transient TBP-2 overexpression suppressed GSIS (Fig. 5c,e). Induction of TBP-2 in cloned INS-1 cells, where TBP-2 expression was doxycycline-off dependent, suppressed GSIS, but not KCl-induced insulin secretion (Fig. 5f,g). TBP-2 induction did not cause a significant change in ATP levels at low (2.8 mM) glucose level, but it suppressed ATP levels at high (16.7 mM) glucose in INS-1 cells (Fig. 5h). Furthermore, glucose-induced intracellular Ca^{2+} elevation, which is the eventual trigger for the exocytosis of insulin granules, was significantly decreased in TBP-2-induced INS-1 cells (Fig. 5i). We then analysed mitochondrial membrane potentials ($\Delta\psi_m$) in TBP-2-induced INS-1 cells. We showed that $\Delta\psi_m$ was significantly reduced in TBP-2-induced INS-1 cells cultured with low (3 mM) and high (20 mM) glucose (Fig. 5j) and with 11 mM glucose for 24 h (Fig. 5k) using a flowcytometer and fluorescence microscopy, respectively. Cellular ATP is mainly produced by glycolysis and mitochondrial metabolism. In pancreatic β-cells, glycolytic flux regulates glucose metabolism, which has an important role in insulin secretion, and glucokinase is a pace-setting enzyme in glycolysis[31]. Therefore, effects of TBP-2 on glucokinase activity were examined. Glucokinase activity

© 2010 Macmillan Publishers Limited. All rights reserved.

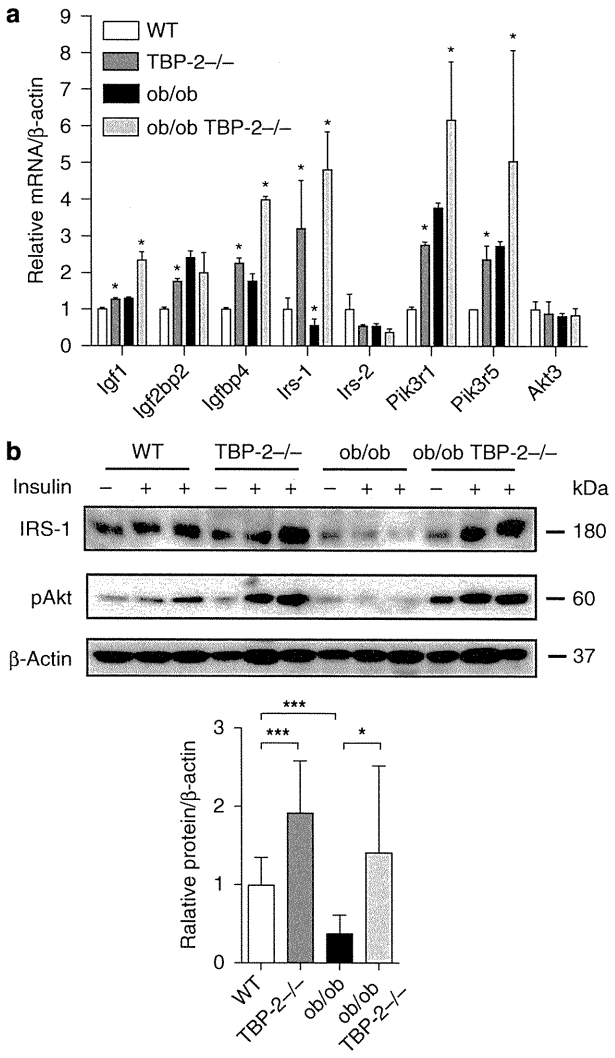

Figure 3 | Insulin signalling-related genes are upregulated by TBP-2 deficiency in skeletal muscle. The expression of insulin signal-related genes from the skeletal muscle of 10 weeks aged WT (white bar), TBP-2−/− (dark grey bar), ob/ob (black bar) and ob/ob·TBP-2−/− (light grey bar) mice. (**a**) Real-time PCR analyses were performed. Asterisk indicates *$P<0.05$;WT versus TBP-2−/−, WT versus ob/ob, ob/ob versus ob/ob·TBP-2−/−. (**b**) Immuno blotting (IB) analyses, *n* per group 3–5 each. Two U kg^{-1} insulin (+) or saline (−) was injected. Densitometric quantification of IRS-1/β-actin is shown in the bar graph. Data are presented as mean±s.d. *$P<0.05$, ***$P<0.001$, versus control (*t*-test).

was not affected by dox-off-dependent TBP-2 induction in β-cells (Fig. 5l). Furthermore, effects of TBP-2 on insulin secretion stimulated by fuel secretagogues, which bypass glycolysis and are metabolized in mitochondria to generate ATP, were determined using methods previously described[32]. Insulin secretion induced by pyruvate and α-ketoisocaprotate plus monomethyl succinate was also suppressed by TBP-2 overexpression in β-cells (Fig. 5m). These results indicate that impaired GSIS by TBP-2 induction is attributable to reduction in mitochondrial metabolism, but not to a decrease in glycolysis.

TBP-2 has been reported to enhance apoptosis in pancreatic β-cells and other cells[21]. TBP-2 induction did not increase apoptosis in 48 h, but apoptosis was slightly increased on 72 h after high (20 mM) glucose treatment (Fig. 5n). β-Cell apoptosis was not changed significantly between ob/ob and ob/ob TBP-2−/− mice generated in a C57BL/6J background at 10 weeks of age (Supplementary Figs S3a,b and S4a), whereas TBP-2 deficiency suppressed β-cell apoptosis at age 36 weeks in C57BL/6J background mice (Supplementary Fig. S4b,c).These results suggest that TBP-2 negatively regulates GSIS by suppressing glucose-induced mitochondrial ATP production in INS-1 cells and islets before causing apoptosis. Treatment with reactive oxygen species scavengers (vitamins C+E) scarcely recovered the insulin secretion suppressed by TBP-2 overexpression in INS-1 cells (Supplementary Fig. S5), suggesting that mitochondrial dysfunction caused by TBP-2 is not mainly attributed to an increase in reactive oxygen species by reducing the scavenger effect of thioredoxin.

TBP-2 enhances UCP-2 transcriptional activity. Impairment in mitochondria ATP production often occurs with uncoupling[24]. Mitochondrial UCP-2 is a key regulator of ATP production and insulin secretion in pancreatic β-cells, and UCP-2 deficiency has been shown to improve GSIS and glucose-induced ATP production in ob/ob mice[24]. Thus, we measured UCP-2 mRNA in TBP-2-overexpressed INS-1 cells. Strikingly, there was a significant increase in UCP-2 mRNA levels in the TBP-2-induced cells (Fig. 6a). Furthermore, TBP-2 induction also increased UCP-2 protein levels in the mitochondria of INS-1 cells (Fig. 6b). UCP-2 expression is known to be upregulated by the increase in activity of transcriptional co-activators; e.g., PPARγ co-activator-1α (PGC-1α)[33]. TBP-2 is also induced by PGC-1α overexpression in INS-1 cells (Fig. 6c). We examined the effect of TBP-2 overexpression on activity of UCP-2 -86 promoter, containing Sp1, SRE and double E-box elements, the essential elements for a response to fatty acids and PGC-1α[33,34]. TBP-2 enhanced UCP-2 transcriptional activity through this -86 promoter region and the PGC-1α-induced activation was also augmented by TBP-2 expression (Fig. 6d), suggesting that TBP-2 enhances UCP-2 transcriptional activity and expression in INS-1 cells. To investigate how TBP-2 regulates UCP-2 transcriptional activity, we tested whether TBP-2 affects PGC-1α protein levels. Dox-off-dependent TBP-2 overexpression did not change PGC-1α protein levels (Supplementary Fig. S6). Next, we used chromatin immunoprecipitations (ChIPs) to investigate whether TBP-2 expression influences PGC-1α binding efficiency to the UCP-2 promoter region. Sheared chromatin was collected from INS-1 cells treated with or without doxycycline, and then immunoprecipitated with anti-RNA polymerase II or control-mouse immunoglobulin G or anti-PGC-1α antibody. PCR was performed with primers flanking the SP1, SRE and E-boxes region of UCP-2 (UCP-2 -86). PGC-1α was recruited to the UCP-2 -86 promoter region and dox-off-dependent TBP-2 overexpression enhanced PGC-1α binding efficiency to the region (Fig. 6e,f). These results indicate that TBP-2 facilitates PGC-1α recruitment in the UCP-2 promoter region, enhancing UCP-2 transcriptional activity in INS-1 cells. Next, we tested whether TBP-2-dependent UCP-2 expression is critical for aggravated GSIS using UCP-2 knockdown in dox-off-dependent TBP-2-overexpressing INS-1 cells. UCP-2 knockdown reversed suppression of GSIS by TBP-2 induction (Fig. 6g and Supplementary Fig. S7), suggesting that TBP-2-induced suppression of GSIS is mainly through UCP-2 expression. Furthermore, the expression level of UCP-2 mRNA was enhanced in islets of ob/ob mice, whereas TBP-2 deficiency dramatically reduced it in ob/ob islets (Fig 6h). Mitochondrial mass, determined as mitochondrial coding gene (mtDNA)/nuclear coding gene (COX I) expression ratio in pancreatic islets, was not affected by TBP-2 deficiency (Fig. 6i). Next, we examined the effect of the mitochondrial uncoupler carbonyl cyanide m-chlorophenyl-hydrazone (cccp) on GSIS in Tet-TBP-2 INS-1 cells with or without doxycycline and in TBP-2 deficient ob/ob islets. Uncoupling by cccp decreased the GSIS at the concentration 25–1,000 nM (Supplementary Fig. S8a). This result suggests that mitochondria metabolism is responsible for GSIS in β-cells and is tightly regulated by uncoupling. In dox-off tet-TBP-2 INS-1 cells, TBP-2 overexpression suppressed the GSIS equivalent

© 2010 Macmillan Publishers Limited. All rights reserved.

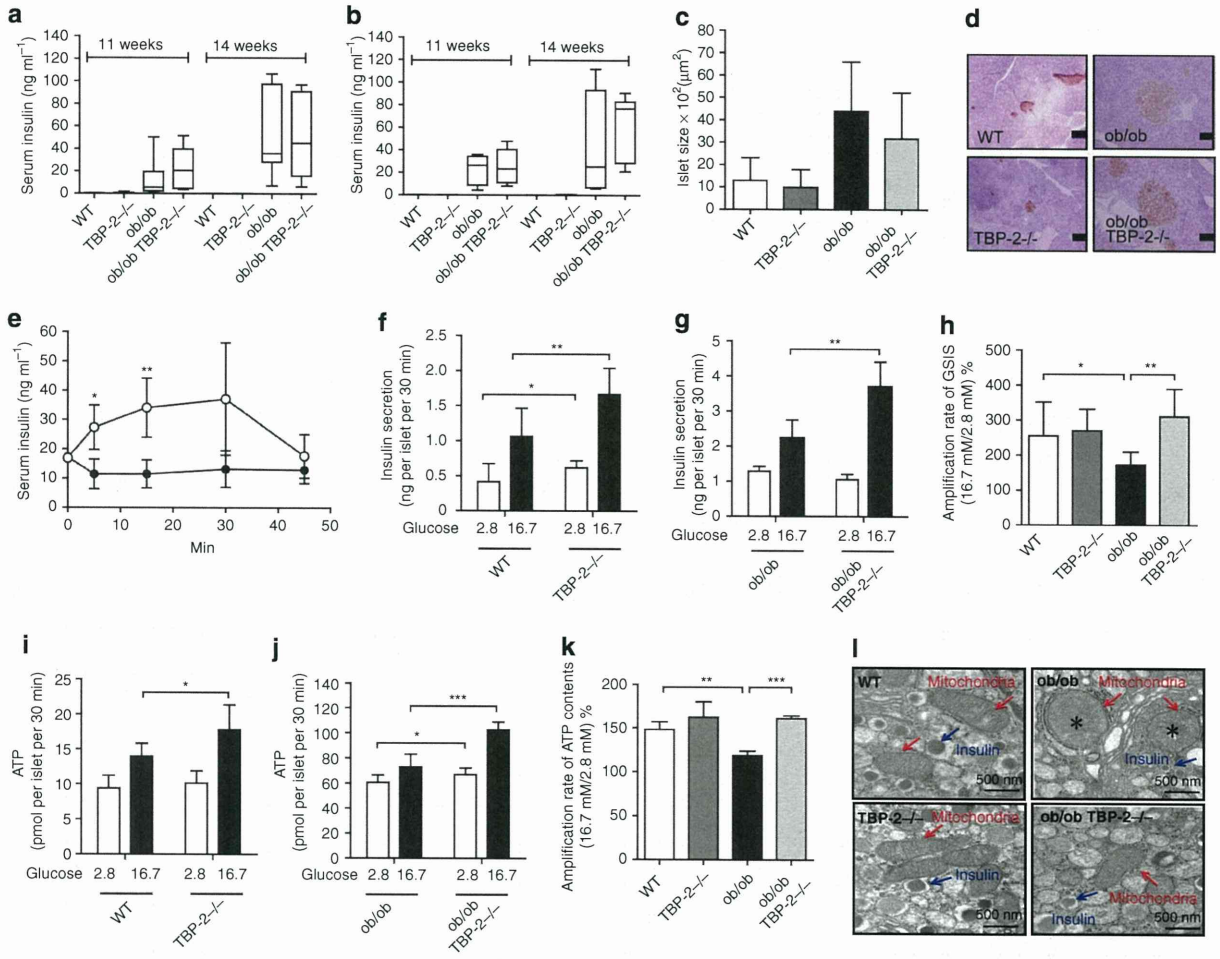

Figure 4 | Impairment of glucose-stimulated insulin secretion in ob/ob mice is improved by TBP-2 deficiency *in vivo* and *ex vivo*. Serum insulin concentrations at 11 and 14 weeks aged male (**a**) and female (**b**) mice. The median lines are shown in box graphs. $n = 6$–12 per group. Physiological analyses of islet mass (**c**) and insulin immunostaining of islets (**d**) in 10 weeks aged mice. Scale bars, 100 μm; $n = 3$ per group. (**e**) Serum insulin levels during intraperitoneal glucose tolerance tests (IPGTTs). Following an overnight fast, mice were injected with 1 g kg^{-1} glucose, IP (time 0). Serum insulin values were assessed before and at 5, 15, 30 and 45 min into the IPGTT. ob/ob (closed circle, $n = 6$), ob/ob·TBP-2 −/− (open circle, $n = 5$). (**f**–**k**) Batches of 10 pancreatic islets isolated from WT, TBP-2 −/−, ob/ob and ob/ob·TBP-2 −/− mice of 10 weeks age were stimulated with 2.8 mM (open bar) or 16.7 mM glucose (closed bar) for 30 min. Insulin secretion (**f**–**h**) and ATP contents (**i**–**k**) were measured by radioimmunoassay and a luminometer, respectively. WT was compared with TBP-2 −/− (**f**, **i**) or ob/ob with ob/ob·TBP-2 −/− (**g**, **j**). Amplification rate of insulin secretion (**h**) and ATP contents (**k**) at high (16.7 mM) glucose compared with basal (2.8 mM) glucose stimulation for 30 min. (**l**) Electron microscopic images of islet sections (×30200; scale bar, 500 nm). Magnified areas of individual β-cell mitochondria. Red arrows highlight individual mitochondria and blue arrows highlight insulin granules. *Swelling and disappearance of cristae structures of mitochondria. Data are presented as mean ± s.d. *$P < 0.05$, **$P < 0.01$, ***$P < 0.001$, versus control (*t*-test).

to the level elicited by 25 nM cccp (Supplementary Fig. S8b). More importantly, cccp had a larger effect on GSIS and glucose-induced ATP production in TBP-2-deficient ob/ob islets compared with ob/ob islets (Fig. 6j,k). These results suggest that TBP-2-dependent regulation of GSIS is mainly achieved through mitochondrial uncoupling and metabolism.

These results suggest that TBP-2 does not affect mitochondrial biogenesis but enhances UCP-2 transcriptional activity through the PGC-1α-dependent pathway, and the induction of the TBP-2-UCP-2 axis causes the defect of GSIS in ob/ob mice.

Mybbp1a is a novel candidate binding protein for TBP-2. To obtain further insight on how TBP-2 regulates gene expression in β-cells, we purified the TBP-2 protein complex using tosyl (p-toluene sulfonyl)-activated magnetic beads (Ts beads). His-tagged-TBP-2 protein was conjugated to the beads and incubated with nuclear extract of INS-1 cells. After washing, the eluate fractions were subjected to SDS gel electrophoresis and silver staining (Fig. 7a). The specific bands on silver staining were subjected to proteolytic digestion and mass spectrometry. Mybbp1a (p160), Mybbp1a (p140), GCN and NonO/p54nrb homologue were identified (Fig. 7b and Supplementary Table S3). Intriguingly, Mybbp1a is reported to inhibit PGC-1α function and transcription of PGC-1α target genes[35]. Therefore, we examined the interaction between TBP-2 and Mybbp1a. We showed that Mybbp1a is detected in elution samples from TBP-2 protein beads by anti-Mybbp1a antibody (Fig. 7c). To determine whether TBP-2 and Mybbp1a interact directly *in vivo*, we performed co-immunoprecipitation using FLAG-HA-tagged Mybbp1a and Myc-tagged TBP-2 expression vectors. Myc-tagged TBP-2 was co-immunoprecipitated with FLAG-HA-tagged Mybbp1a in HEK293 cells (Fig. 7d). Finally, we examined whether Mybbp1a regulates UCP-2 transcriptional activity. Mybbp1a suppressed PGC-1α-dependent UCP-2 transcriptional activity and the suppression was reversed by TBP-2

© 2010 Macmillan Publishers Limited. All rights reserved.

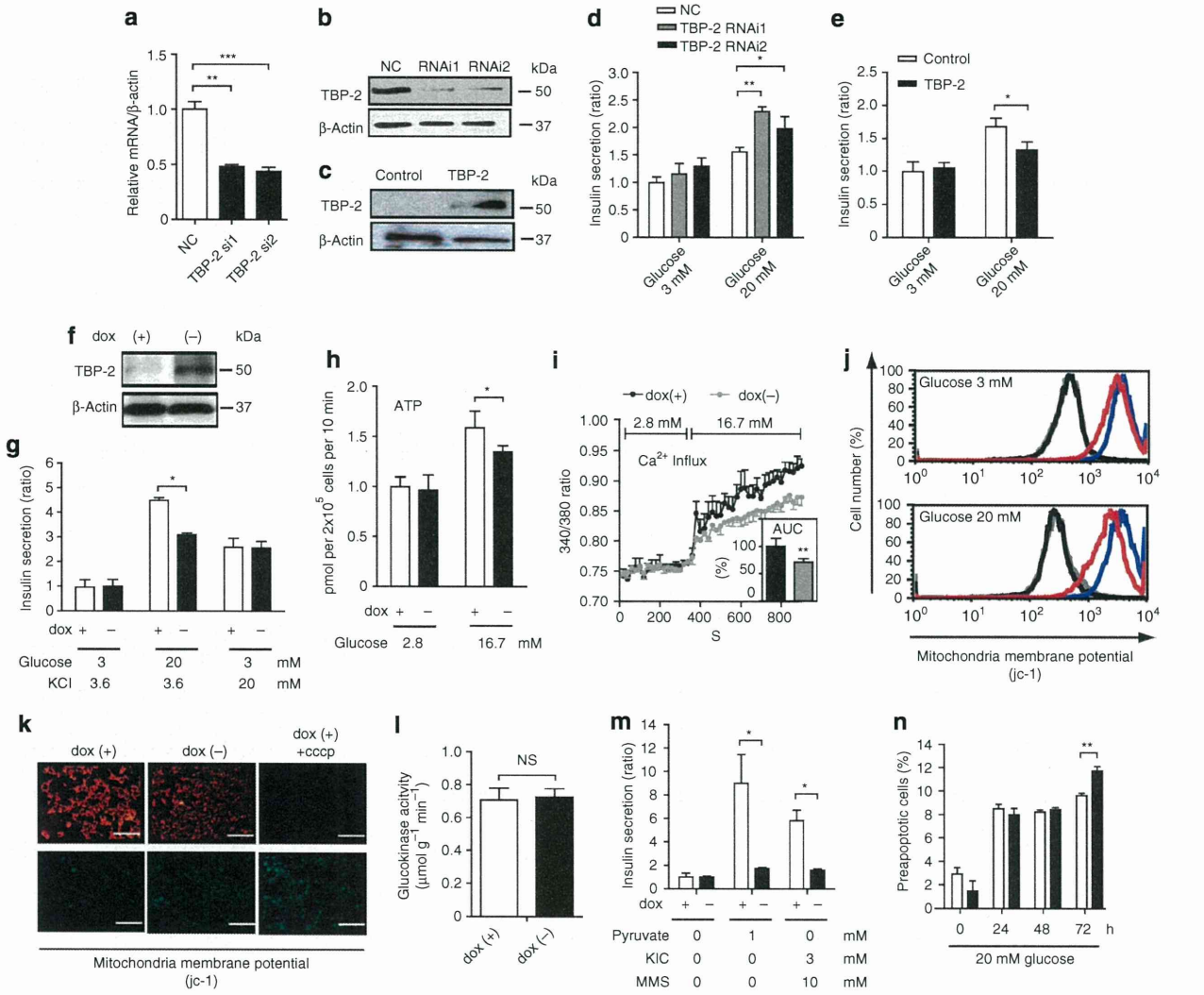

Figure 5 | TBP-2 suppresses glucose-induced mitochondrial energy production and insulin secretion in β-cells. Transient TBP-2 knockdown by TBP-2 siRNA (RNAi1 and RNAi2) and negative control siRNA (NC) in INS-1 cells. The expression of TBP-2 was determined by qRT-PCR (**a**) at 48 h after transfection and by immunoblot analysis (**b**) at 72 h after transfection. (**c**) Transient TBP-2 overexpression in INS-1 cells after 24 h. The expression of TBP-2 was determined by immunoblot analyses. Augmentation or suppression of GSIS in TBP-2 knockdown (**d**) or TBP-2 overexpression (**e**) cells in RPMI cultured medium. Statistic insulin secretion assays were analysed in INS-1 cells. (**f**) Construction of the doxycycline (dox)-off-dependent TBP-2-overexpressed INS-1 cells. TBP-2 protein was suppressed by 1000 ng ml^{-1} dox and induced by dox removal. Cells were cultured with (+, open bar) or without (−, closed bar) dox for 24 h. INS-1 cells were incubated at low (2.8 or 3 mM) or high (16.7 or 20 mM) glucose and experiments were performed. Suppression of high (20 mM) GSIS (**g**), high (16.7 mM) glucose-enhanced ATP contents (**h**) and intracellular Ca^{2+} influx (**i**) by dox-off TBP-2 overexpression, but not KCl-induced insulin secretion (**g**). The inset bar graph shows area under the curve levels (%) of intracellular Ca^{2+} levels between 320 and 900 s (**i**). Decrease of mitochondrial membrane potentials (MMP) in dox-off TBP-2 overexpression in INS-1 cells. MMP of cultured cells in medium containing 3 mM (upper panel) or 20 mM (lower panel) glucose for 24 h was analysed by flow cytometry (**j**) or in cultured medium by fluorescence microscopy (**k**) using jc-1 reagent, scale bar is 100 μm. For disruption of MMP, 5 μM carbonyl cyanide m-chlorophenlhydrazone (cccp) reagent was used. Flow cytometer, blue; dox (+), red; dox (−), black; dox (+) + cccp, grey; dox (−) + cccp. (**l**) Glucokinase (GK) activities in INS-1 cells, NS, nonsignificant. (**m**) Suppression of pyruvate (sodium pyruvate) or 2-ketoisohexanoic acid (KIC) and methylsaccinic acid (monomethyl succinate)-stimulated insulin secretion by dox-off-dependent TBP-2 overexpression. (**n**) A flow cytometric analyses with Annexin V-fluorescein isothiocyanate and propidium iodide staining in the dox-off TBP-2-overexpressed INS-1 cells. Preapoptotic cells were calculated from triplicate samples (%). Data are presented as mean ± s.d. *P < 0.05, **P < 0.01, ***P < 0.001, versus control (t-test).

co-expression (Fig. 7e). These results provide a model that TBP-2 suppresses Mybbp1a function possibly through protein–protein interaction, leading to the activation of PGC-1α-dependent UCP-2 transcription (Fig. 7f).

Discussion

In this study, we demonstrated that disruption of TBP-2 expression augments both insulin sensitivity and secretion, resulting in the amelioration of glucose intolerance in a diabetic mice model where TBP-2 expression is increased. The mechanism by which TBP-2 is increased in several tissues and pancreatic islets of ob/ob mice is presently unknown. It is possible that high blood glucose or obese-induced adipocytokines enhance TBP-2 expression, as TBP-2 is upregulated by several stimulations and stresses[36,37]. Several reports have shown that TBP-2 expression is regulated by mitochondrial metabolism and glycolysis through the transcription factor

© 2010 Macmillan Publishers Limited. All rights reserved.

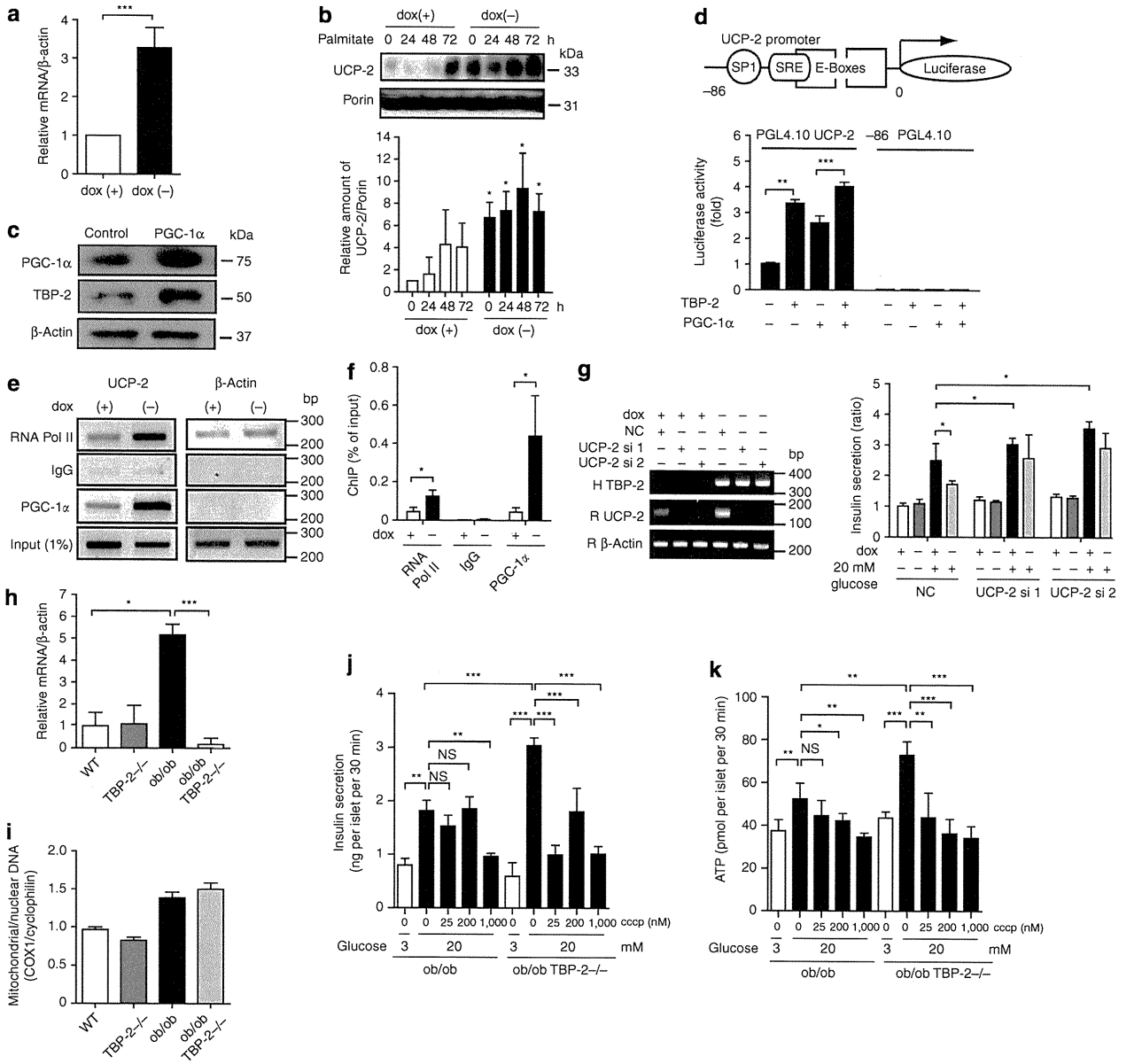

Figure 6 | TBP-2 enhances UCP-2 transcriptional activity. (**a**) Quantitative RT-PCR (qRT-PCR) analyses of UCP-2 mRNA expression in dox-off-dependent TBP-2-overexpressed INS-1 cells with or without dox. (**b**) Immuno blotting to determine UCP-2 expression in mitochondria in dox-off TBP-2 overexpression in INS-1 cells with or without palmitate (300 μM) for the indicated time. Densitometric quantification of the UCP-2/Porin ratio in mitochondria of INS-1 cells is shown in a bar graph. (**c**) Immuno blotting analyses to detect expression of PGC-1α, TBP-2 and β-actin in INS-1 cells, transiently transfected with PGC-1α plasmid for 24 h. (**d**) INS-1 cells were transfected with PGL4.10 UCP-2 -86 or PGL4.10-luciferase reporter plasmid and each expression plasmid for PGC-1α and TBP-2, as indicated. Luciferase reporter activity was normalized by *Renilla* luciferase activity. (**e**) ChIP assay of PGC-1α protein binding to endogenous *UCP-2* promoter. Chromatin extracts from INS-1 cells in dox-off-dependent TBP-2-overexpressed INS-1 cells with or without dox were precipitated in the presence of control-mouse IgG, anti-RNA polymerase II (RNA pol II) or anti-PGC-1α antibody. Primers for PCR are rat *UCP-2* promoter region primers and rat *β-actin* primers. (**f**) qRT-PCR analyses for ChIP were performed. (**g**) Insulin secretion in dox-off-dependent TBP-2 overexpressing INS-1 cells with or without dox and knockdown of UCP-2 (si1 and si2). The left panel shows RT-PCR analysis of human *TBP-2* expression (H TBP-2) to confirm the effect of dox, rat *UCP-2* expression (R UCP-2) to confirm the knockdown effect, and rat *β-actin* (R β-actin). (**h**) qRT-PCR analyses of UCP-2 mRNA in isolated pancreatic islets of WT, TBP-2 −/−, ob/ob and ob/ob·TBP-2 −/− mice. (**i**) qRT-PCR was used to determine mitochondria content by measuring the expression of mitochondrial gene (COX I)/nuclear gene (cyclophilin) ratios. (**j**, **k**) Effect of cccp treatment for 30 min on insulin secretion (**j**, ng per islet per 30 min) and ATP levels (**k**, pmol per islet per 30 min) in ob/ob and ob/ob TBP-2 −/− islets. Data are presented as mean ± s.d. $^{*}P<0.05$, $^{**}P<0.01$, $^{***}P<0.001$, versus control (*t*-test).

MondoA[38–41]. These reports indicate that TBP-2 expression is tightly regulated in response to changes in energy status.

TBP-2 deficiency in ob/ob mice improved hyperglycaemia, glucose intolerance and insulin resistance without amelioration of obesity (Fig. 1e–m). A previous study showed that HcB-19 mice crossed with ob/ob mice improved glucose tolerance[21]. Other studies showed that silencing of TBP-2 expression enhanced glucose uptake in adipocytes and human skeletal myocytes, whereas TBP-2 overexpression

© 2010 Macmillan Publishers Limited. All rights reserved.

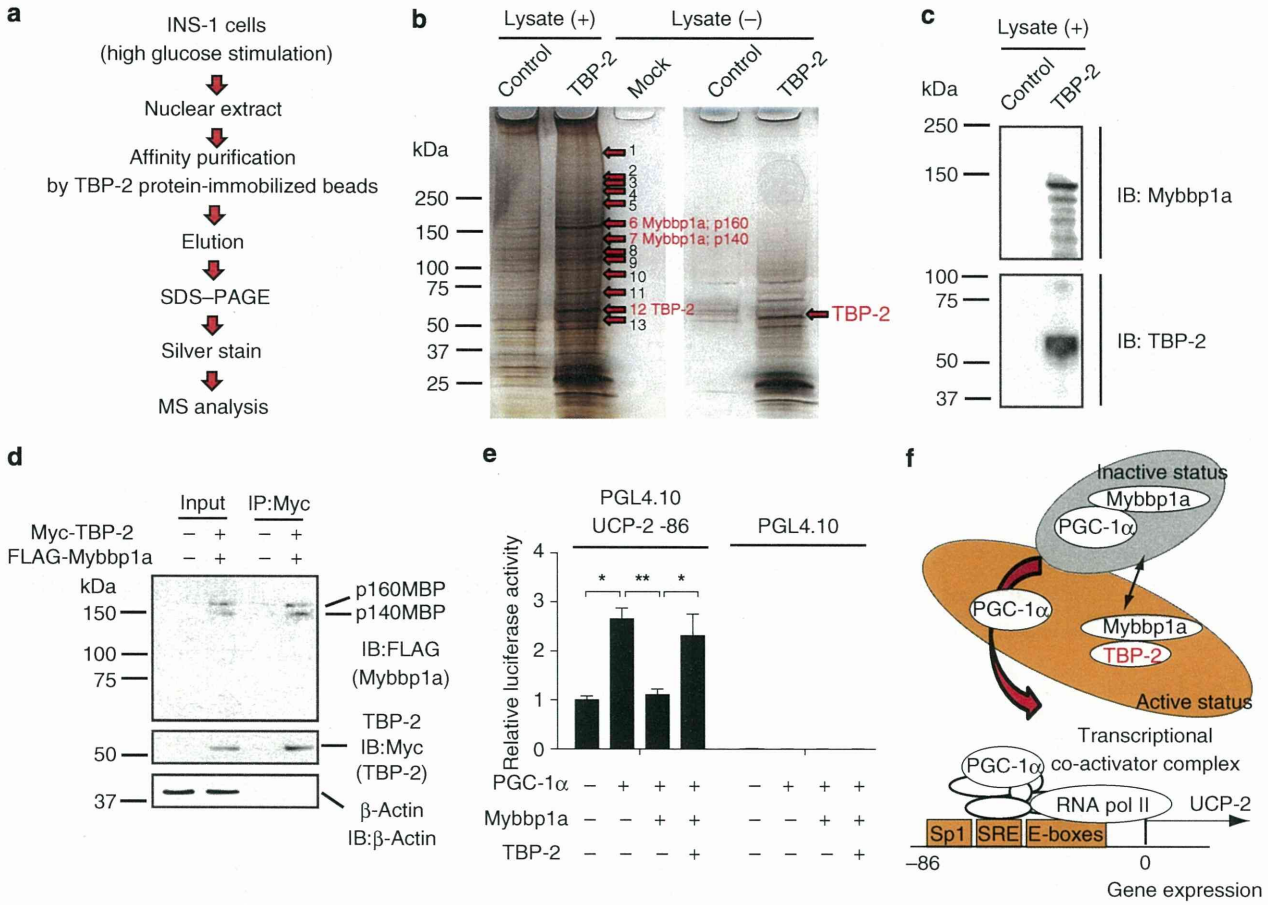

Figure 7 | Mybbp1a was identified as a novel candidate binding protein for TBP-2. (**a**) Purification scheme for the TBP-2 containing protein complex in β-cell nuclear extracts. TBP-2 binding proteins were purified from INS-1 nuclear extracts by using TBP-2 protein-immobilized (TBP-2) or control beads. (**b**) Identification of the TBP-2 complex. Silver staining was performed. Numbers indicate individual candidate proteins interacting with TBP-2. (**c**) Eluted proteins were analysed by immuno blotting (IB) for Mybbp1a and TBP-2 antibody. (**d**) Co-immunoprecipitation analyses. Input (left, 5% lysate) and anti-Myc immunoprecipitates (right, IP:Myc) from HEK293 cells transfected with pCMV-tag2A and pCMV-tag3B vector (−) or FLAG-HA-Mybbp1a and Myc-TBP-2 vector (+) were analysed by immunoblotting (IB) with antibodies to FLAG, Myc and β-actin. The positions for Mybbp1a (p160; p160MBP) and Mybbp1a (p140; p140MBP) (upper), TBP-2 (middle) and β-actin (lower) are shown. (**e**) Luciferase activity of the UCP-2 -86 enhancer region. INS-1 cells were transfected with PGL4.10 UCP-2 -86 or PGL4.10-luciferase reporter plasmid and each expression plasmid for PGC-1α, Mybbp1a and TBP-2, as indicated. Luciferase reporter activity was normalized by *Renilla* luciferase activity. (**f**) A schematic model of TBP-2 function in β-cells. Mybbp1a binds PGC-1α (inactive form) and inhibits UCP-2 transcriptional activity. Induced TBP-2 interacts with Mybbp1a and releases PGC-1α from Mybbp1a, facilitating PGC-1α recruitment on the UCP-2 promoter region. Data are presented as mean±s.d. $^{*}P<0.05$, $^{**}P<0.01$, versus control (*t*-test).

inhibited glucose uptake[19]. Entire or muscle-specific TBP-2−/− mice showed enhanced glucose uptake in the skeletal muscle and adipose with a high-fat diet[23,42]. The current study is consistent with these previous reports. The restoration of glucose tolerance in ob/ob·TBP-2−/− mice could not be explained by changes in energy balance or hormonal level of adipocytokines, such as adiponectin, free fatty acids and MCP-1. Insulin resistance in skeletal muscle and liver is mainly caused by inactivation of insulin/Akt signalling[1]. We showed that TBP-2 deficiency in ob/ob mice improved Akt signalling in muscle but not liver (Fig. 2k–p). Moreover, *IRS-1* gene and several insulin signalling genes were upregulated in skeletal muscle by TBP-2 deficiency both in WT and ob/ob mice (Fig. 3a and Supplementary Table S2). IRS-1 protein levels were downregulated in the skeletal muscle of ob/ob mice compared with that of WT mice, while IRS-1 protein levels were also upregulated by TBP-2 deficiency in both WT and ob/ob mice (Fig. 3b). As IRS-1 has a pivotal role in insulin sensitivity in muscle[27], TBP-2 regulates insulin signalling possibly through the regulation of *IRS-1* gene expression in muscle. Interestingly, TBP-2 deficiency did not change *IRS-2* gene expression, which is known as a main regulator of liver insulin sensitivity[43] in skeletal muscle (Fig. 3a). These results suggest that TBP-2 regulates IRS-1-related insulin sensitivity in skeletal muscle, but not IRS-2-related insulin sensitivity in liver. The molecular mechanism of how TBP-2 regulates the expression of IRS-1 and insulin signalling genes in skeletal muscle is now under investigation. We also found that gene expression of PPARs and their target genes, such as *PPARγ*, *PPARα*, *Acaca*, *Fabp3*, *Scd1* and *Pdk4*, are enhanced by TBP-2 deficiency in skeletal muscle (Supplementary Fig. S2), similar to previous reports in the liver and adipose tissue of TBP-2−/− mice[16,42]. As PPAR signalling augments insulin sensitivity[44], it may also be involved in enhanced insulin sensitivity by TBP-2 deficiency.

The GSIS was significantly impaired in ob/ob islets, whereas insulin secretion from ob/ob·TBP-2−/− islets was restored *in vivo* and *ex vivo*, suggesting that the ablation of TBP-2 in pancreatic islets of ob/ob mice augments GSIS. Our results indicate that upregulation of TBP-2 suppresses GSIS by reducing ATP production in pancreatic β-cells. Meanwhile, glycolytic activity was not changed by TBP-2 overexpression (Fig. 5l) in β-cell lines. Recently, several groups have

© 2010 Macmillan Publishers Limited. All rights reserved.

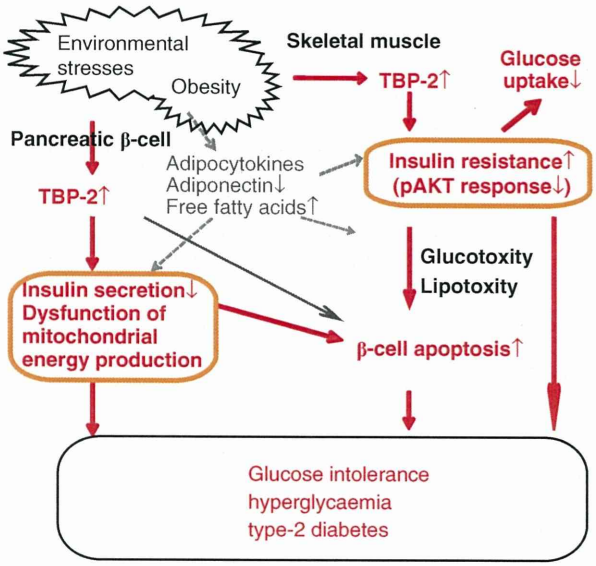

Figure 8 | A model for metabolic function of TBP-2 in diabetes. Role of TBP-2 in promoting obesity-induced type 2 diabetes. Environmental stresses including obesity cause upregulation of TBP-2. Sustained expression of TBP-2 may impair mitochondrial function and insulin secretion in β-cells and aggravate insulin resistance in skeletal muscle. Augmented expression of TBP-2 may also result in β-cell apoptosis. These changes lead to glucose intolerance and hyperglycaemia and obese-induced type 2 diabetes.

shown that TBP-2 regulates β-cell mass and β-cell apoptosis in C3H/He background mice and INS-1 cells[21,22,45,46]. Our results also support these previous studies. TBP-2 deficiency suppressed β-cell apoptosis at age 36 weeks in C57BL/6J background mice (Supplementary Fig. S4b,c). In contrast, while β-cell apoptosis was not changed significantly between ob/ob and ob/ob·TBP-2−/− mice generated in C57BL/6J background mice at 10 weeks age (Supplementary Figs S3a,b and S4a,c), TBP-2 deficiency improved GSIS in ob/ob mice at age 10–14 weeks. Taken together, improvement of GSIS by TBP-2 depletion *in vivo* was attributable to functional amelioration of β-cells but not to an increase in β-cell mass, at least, in mice of this age. Moreover, impaired GSIS without reduction in β-cell mass preceded significant detection of apoptosis in islets in ob/ob mice, which supports the pathogenic importance of functional impairment of β-cells. Thus, TBP-2 seems to regulate not only β-cell apoptosis but also β-cell energy metabolism in the diabetic condition.

Impairment of GSIS in ob/ob mice was improved by TBP-2 deficiency. This phenotype resembles ob/ob mice lacking UCP-2, which is a negative regulator of GSIS[24]. We showed that TBP-2 deficiency cancelled upregulation of UCP-2 gene expression in ob/ob islets (Fig. 6h). Therefore, UCP-2 regulation by TBP-2 seems to be important in the development of the diabetic phenotype in ob/ob mice. UCP-2 knockdown recovered the TBP-2-dependent impairment in GSIS (Fig 6g). Furthermore, the mitochondrial uncoupling reagent cccp had a greater effect on GSIS and glucose-induced ATP production in TBP-2-deficient ob/ob islets compared with those in ob/ob islets (Fig. 6j,k). These results suggest that TBP-2-dependent regulation of GSIS is mainly due to mitochondrial uncoupling derived from UCP-2 expression.

The results from a ChIP assay indicated that TBP-2 regulates UCP-2 expression by facilitating PGC-1α recruitment to the UCP-2 promoter region. Furthermore, we identified Mybbp1a as a novel binding protein of TBP-2. Mybbp1a is reported to inhibit PGC-1α function and transcription of PGC-1α target genes through direct protein–protein interaction[35]. Indeed, Mybbp1a overexpression suppressed PGC-1α-dependent UCP-2 transcriptional activity (Fig. 7e), and TBP-2 overexpression hampered the effect of Mybbp1a on PGC-1α-dependent UCP-2 promoter activity in INS-1 cells (Fig. 7e). These results suggest a model that TBP-2 regulates UCP-2 expression through Mybbp1a and PGC-1α pathway (Fig. 7f). Recently, it has been reported that α-arrestin family proteins are considered to act as adaptor protein for the E3-ubiquitin ligases in the yeast system[47] and TBP-2 interacts with WW domain of HECT domain containing E3-ubiquitin ligases through the PPxY motif of TBP-2[12]. These reports provide a hypothesis that TBP-2 negatively regulates Mybbp1a by protein degradation through E3-ubiquitin ligases. This possibility should be further investigated.

In this study, we demonstrated that ablation of TBP-2 expression augments both insulin sensitivities by enhancing IRS-1/Akt signalling in skeletal muscle and GSIS by suppressing UCP-2 transcription and maintaining mitochondrial function in pancreatic β-cells, resulting in the amelioration of glucose intolerance and hyperglycaemia. The proposed mechanism for this effect is summarized in Figure 8 and Supplementary Figure S9. These findings raise the possibility that the inhibition of either TBP-2 activity or expression may be a novel therapeutic approach for type 2 diabetes.

Methods

Animal experiments. TBP-2-knockout mice were generated as described previously[17]. Mice were backcrossed for at least 11 generations with a C57B/6 genetic background. Animals were maintained in a specific pathogen-free animal facility on a 12-h light–dark cycle at an ambient temperature of 21 °C. They were given free access to water and food.

Age- and sex-matched mice were used for all animal experiments. All procedures involving animals were performed in accordance with protocols approved by the Animal Care and Research Advisory Committee of the Institute for Virus Research at Kyoto University.

Generation of TBP-2-deficient ob/ob mice. C57BL6 ob/+ were purchased from the Jackson Laboratory. To generate ob/ob·TBP-2−/− mice, TBP-2−/− mice were crossed with ob/+ mice creating compound heterozygotes, ob/OB·TBP-2+/−. In the second cross, compound heterozygotes were crossed to generate the following animals of which both males and females were collected and studied further: WT mice (+/+ at both ob and TBP-2 loci), ob/ob mice (ob/ob at the ob locus and +/+ at the TBP-2 locus), TBP-2−/− mice (+/+ at the ob locus and −/− at the TBP-2 locus) and ob/ob·TBP-2−/− mice (ob/ob at the ob locus and −/− at the TBP-2 locus). The ob allele was genotyped as previously described[48].

Intraperitoneal glucose or ITTs. For the intraperitoneal (IP) glucose tolerance test, following an overnight fast, ob/ob and ob/ob·TBP-2−/− mice were injected with 0.5 g kg^{-1} or 1 g kg^{-1} glucose. Blood glucose values were assessed before and at 15, 30, 60 and 120 min after the IP administration of glucose using glucose PILOT. Serum insulin values were assessed before and at 5, 15, 30 and 45 min after the IP administration of glucose using an Insulin ELISA kit. For the IP ITTs, mice were fasted for 6 h and then injected with 1 U kg^{-1} insulin.

Cell culture and transfection. INS-1 cells were cultured at 37 °C with 5% CO_2 in air in RPMI1640 (Sigma-Aldrich), supplemented with 10% (v/v) fetal bovine serum, 1% (v/v) penicillin/streptomycin antibiotics, 10 mM HEPES, 2 mM L-glutamine, 1 mM sodium pyruvate and 50 μM β-mercaptoethanol (RPMI for INS-1 medium). INS-1 cells were transfected with TBP-2 small interfering RNA (siRNA) or negative control siRNA (Qiagen) for 72 h or with pCMV-Tag2B-TBP-2 or control pCMV-Tag2B (Stratagene) plasmid for 24 h and cultured with RPMI1640 for INS-1 medium.

Isolated pancreatic islet studies. Pancreatic islets were isolated from mice according to a method used for rats[49].

Generation of INS-1 cells with inducible TBP-2 expression. Stable INS-1 cells, which carry the reverse tetracycline/doxycycline-dependent transactivator pTRE2 (pTet-Off, Clontech), were prepared. After selection with 500 μg ml^{-1} G418, resistant colonies were isolated with limiting dilution methods in 96-well plates. One clonal line that exhibited very high tetracycline-off-inducible luciferase activity and undetectable basal luciferase activity was chosen and used for a second round of transfection with the TBP-2 expression plasmid (pTRE2 pur-TBP-2-FLAG). After selection with 500 ng ml^{-1} puromycin and doxycycline-off-induced TBP-2 expression, clones were isolated.

Insulin secretion assay using INS-1 cells. INS-1 cells were transfected with TBP-2 siRNA (Rn_Txnip_1 and 5) or UCP-2 siRNA (Rn_UCP-2_5 and 6) or negative control siRNA (purchased from Qiagen) for 72 h, or with pCMV-Tag2A-TBP-2 or

© 2010 Macmillan Publishers Limited. All rights reserved.

control pCMV-Tag2A (Stratagene) plasmid for 24 h. Then, the cells were cultured in Krebs Ringer bicarbonate buffer (KRBB) (as mentioned below) or RPMI1640 for INS-1 medium with 2.8 mM (5 mM) or 16.7 mM (20 mM) glucose containing RPMI medium and the supernatant was collected 30 min after the addition of glucose. Insulin concentration was measured by an Insulin ELISA kit. Similar analyses were performed in Tet-TBP-2 INS-1 cells pretreated with or without doxycycline for 24 to 48 h. One mM pyruvate (sodium pyruvate, Nacalai Tesque) or 3 mM α-ketoisocaprotate (2-ketoisohexanoic acid, Nacalai Tesque) and 10 mM monomethyl succinate (methylsuccinic acid sodium salt, Sigma-Aldrich)-stimulated insulin secretion assays were performed in Tet-TBP-2 INS-1 cells.

Insulin secretion assay using primary mouse pancreatic islet. Insulin release from intact islets was monitored using batch incubation methods[50]. Isolated pancreatic islets were precultured at 37 °C for 30 min with gentle swinging (50 times per min) in KRBB containing 129.4 mM NaCl, 3.7 mM KCl, 2.7 mM $CaCl_2$, 1.3 mM KH_2PO_4, 1.3 mM $MgSO_4$, 24.8 mM $NaHCO_3$ (equilibrated with 5% CO_2, 95% O_2, pH 7.4), and 0.2 % (vol/vol) bovine serum albumin (fraction V) with 2.8 mM glucose. Next, the pancreatic islets were incubated for 30 min in KRBB buffer with glucose 2.8 or 16.7 mM to determine insulin secretion levels. At the end of the incubation period, islets were pelleted by centrifugation, and aliquots of the buffer were sampled. The amount of immunoreactive insulin was determined by radioimmunoassay, using rat insulin as standard.

ATP contents assay. INS-1 cells (2.0×10^5 cells per 24-well plate) or isolated pancreatic islets were precultured in KRBB buffer with 2.8 mM glucose for 2 h or 30 min, and were batch incubated for 10 or 30 min in KRBB with 2.8 or 16.7 mM glucose, respectively. After immediate addition of $HClO_4$, cells were sonicated in ice-cold water for 10 min, and centrifuged. Part of the supernatant fraction was mixed with HEPES and Na_2CO_3 and the ATP content in the cells was determined by luminometer as previously described[50].

Intracellular Ca^{2+} assay. INS-1 cells were precultured for 2 h in KRBB with 2.8 mM glucose and then cells were loaded with 5 μM Fura-PE3 AM in KRBB containing 2.8 mM glucose and 0.2% bovine serum albumin at 37 °C for 20 min. Intracellular Ca^{2+} concentration was measured by the ratio of emission fluorescence of 510 nm by excitation at 340 and 380 nm as previously described[50].

Measurement of mitochondrial membrane potentials. Briefly, INS-1 cells were preincubated in KRBB with 3 and 20 mM glucose or in cultured medium for 24 h, and the cells were resuspended in 0.5 ml of ice-cold PBS, then cultured with 10 nM jc-1 (Sigma-Aldrich, J-4519) for 15 min in 5% CO_2 at 37 °C with or without 5 μM cccp, a protonophore that completely dissipated $\Delta\psi$, and was analysed by flow cytometry (FACSCanto II, BD Bioscience) or fluorescence microscopy (Biozero, Keyence). The greater the mitochondrial membrane potential, the more jc-1 aggregates form that have a red fluorescent emission signal, as opposed to the jc-1 monomer that fluorescences green. Data acquisition and analysis were performed using Cell Quest Software.

Luciferase reporter assays. INS-1 cells were transiently transfected with pGL4.10 luc2 vectors containing UCP-2 -86 enhancer region (5′-GGCTCCGCCTCGT CACGCCACGCCCCGACCACGCCCTCTAGA-3′) or pGL4.10 luc2 vectors, with the pCMV-PGC-1α, pCMV-Tag2A-TBP-2 and FLAG-HA-p160 MBP plasmids. FLAG-HA-p160 MBP was kindly provided by Dr Shunsuke Ishii. As a control, the total amount of vectors for transfection was adjusted by the amount of the pCMV-Tag2A vector. After 18 h of transfection, luciferase activity was quantified using the luciferase assay system (Promega). pRL-TK (Promega) was used to monitor *Renilla* luciferase gene expression as a control for the efficiency of transfection.

Cell culture of primary MEFs. Primary MEFs were derived from 13.5-day-old embryos from TBP-2 +/− mice, and then the MEFs were genotyped to obtain TBP-2 −/− and TBP-2 +/+ MEFs. Cells were maintained in DMEM with 10% fetal calf serum, 1% penicillin and 0.5% L-glutamine. TBP-2 mRNA expression was confirmed by semiquantitative RT–PCR analysis. Primer sequences are listed in Supplementary Table S4.

Quantitative (semiquantitative) RT-PCR analysis. Total RNA was extracted from INS-1 cells or handpicked freshly isolated islets using TRIzol reagent (Invitrogen). Reverse transcription was performed with SuperScript III (Invitrogen) or PrimeScript RT (TAKARA). Real-time RT–PCR was performed using SYBR Premix Ex Tag II(TAKARA). The internal control used was β-actin. PCR analyses were carried out using the oligonucleotide primers listed in Supplementary Table S4.

Chromatin immunoprecipitation. Chromatin was prepared from Tet-TBP-2 INS-1 cells treated with or without doxycycline. Briefly, 5×10^6 cells were crosslinked with 1% formaldehyde for 10 min, followed by the addition of glycine at 125 mM. Chromatin was sheared by enzymes (CHIP IT Express Kit, Active Motif). Chromatin was immunoprecipitated with 2 μg anti-RNA polymerase II (Active Motif), control-mouse immunoglobulin G (Active Motif) or anti-PGC-1α antibodies (Santa Cruz). GATCTGAGACAGGGAGACTCTAGG and GGAGAATACACA GGAGAACACAGG primers were used to amplify the UCP-2 SP1, SRE, E-boxes region. Rat β-actin enhancer primers (Active Motif) were used as control. PCR was carried out with one cycle at 95 °C for 2 min; 36 cycles at 94 °C for 10 s, 60 °C for 30 s, 68 °C for 1 min; and one cycle at 68 °C for 5 min.

Co-immunoprecipitation. To investigate interactions between TBP-2 and Mybbp1a *in vivo*, Myc-TBP-2 and FLAG-HA-Mybbp1a or pCMV-tag3B and pCMV-tag2A (as control) were co-expressed in HEK293 cells. Cells were lysed in lysis buffer (CellLytic M Cell Lysis Reagent, Sigma-Aldrich), and insoluble materials were precipitated by centrifugation at $15,000 \times g$ for 15 min. The resulting supernatants were incubated with anti-Myc agarose beads (MBL), and bound material was eluted with Myc-peptide (500 μg ml^{-1}, MBL). Protein–protein interaction was assessed by immunoblotting using anti-FLAG antibody (Sigma-Aldrich) or anti-Myc antibody (Sigma-Aldrich).

Statistical method. Results were expressed as the mean ± s.d. Statistical comparisons were made using Student's *t*-test. A statistically significant difference was defined as $^*P < 0.05$, $^{**}P < 0.01$, $^{***}P < 0.001$.

References

1. Biddinger, S. B. & Kahn, C. R. From mice to men: insights into the insulin resistance syndromes. *Annu. Rev. Physiol.* **68,** 123–158 (2006).
2. Guilherme, A., Virbasius, J. V., Puri, V. & Czech, M. P. Adipocyte dysfunctions linking obesity to insulin resistance and type 2 diabetes. *Nat. Rev. Mol. Cell Biol.* **9,** 367–377 (2008).
3. Pratley, R. E. & Weyer, C. The role of impaired early insulin secretion in the pathogenesis of Type II diabetes mellitus. *Diabetologia* **44,** 929–945 (2001).
4. Anello, M. *et al.* Functional and morphological alterations of mitochondria in pancreatic beta cells from type 2 diabetic patients. *Diabetologia* **48,** 282–289 (2005).
5. Maechler, P. & Wollheim, C. B. Mitochondrial function in normal and diabetic beta-cells. *Nature* **414,** 807–812 (2001).
6. Bodnar, J. S. *et al.* Positional cloning of the combined hyperlipidemia gene Hyplip1. *Nat. Genet.* **30,** 110–116 (2002).
7. Chen, K. S. & DeLuca, H. F. Isolation and characterization of a novel cDNA from HL-60 cells treated with 1,25-dihydroxyvitamin D-3. *Biochim. Biophys. Acta.* **1219,** 26–32 (1994).
8. Nishiyama, A. *et al.* Identification of thioredoxin-binding protein-2/vitamin D(3) up-regulated protein 1 as a negative regulator of thioredoxin function and expression. *J. Biol. Chem.* **274,** 21645–21650 (1999).
9. Nishinaka, Y. *et al.* Importin alpha1 (Rch1) mediates nuclear translocation of thioredoxin-binding protein-2/vitamin D(3)-up-regulated protein 1. *J. Biol. Chem.* **279,** 37559–37565 (2004).
10. Oka, S. *et al.* Thioredoxin-binding protein-2-like inducible membrane protein is a novel vitamin D3 and peroxisome proliferator-activated receptor (PPAR)gamma ligand target protein that regulates PPARgamma signaling. *Endocrinology* **147,** 733–743 (2006).
11. Patwari, P. *et al.* Thioredoxin-independent regulation of metabolism by the alpha-arrestin proteins. *J. Biol. Chem.* **284,** 24996–5003 (2009).
12. Zhang, P. *et al.* The ubiquitin ligase itch regulates apoptosis by targeting thioredoxin-interacting protein for ubiquitin-dependent degradation. *J. Biol. Chem.* **285,** 8869–79 (2010).
13. Zhou, R., Tardivel, A., Thorens, B., Choi, I. & Tschopp, J. Thioredoxin-interacting protein links oxidative stress to inflammasome activation. *Nat. Immunol.* **11,** 136–140 (2010).
14. Nishinaka, Y. *et al.* Loss of thioredoxin-binding protein-2/vitamin D3 up-regulated protein 1 in human T-cell leukemia virus type I-dependent T-cell transformation: implications for adult T-cell leukemia leukemogenesis. *Cancer Res.* **64,** 1287–1292 (2004).
15. Lee, K. N. *et al.* VDUP1 is required for the development of natural killer cells. *Immunity* **22,** 195–208 (2005).
16. Oka, S. *et al.* Thioredoxin binding protein-2/thioredoxin-interacting protein is a critical regulator of insulin secretion and peroxisome proliferator-activated receptor function. *Endocrinology* **150,** 1225–1234 (2009).
17. Oka, S. *et al.* Impaired fatty acid utilization in thioredoxin binding protein-2 (TBP-2)-deficient mice: a unique animal model of Reye syndrome. *FASEB J.* **20,** 121–123 (2006).
18. Hui, T. Y. *et al.* Mice lacking thioredoxin-interacting protein provide evidence linking cellular redox state to appropriate response to nutritional signals. *J. Biol. Chem.* **279,** 24387–24393 (2004).
19. Parikh, H. *et al.* TXNIP regulates peripheral glucose metabolism in humans. *PLoS Med.* **4,** e158 (2007).
20. Chutkow, W. A., Patwari, P., Yoshioka, J. & Lee, R. T. Thioredoxin-interacting protein (Txnip) is a critical regulator of hepatic glucose production. *J. Biol. Chem.* **283,** 2397–2406 (2008).
21. Chen, J. *et al.* Thioredoxin-interacting protein deficiency induces Akt/Bcl-xL signaling and pancreatic beta-cell mass and protects against diabetes. *FASEB J.* **22,** 3581–3594 (2008).
22. Chen, J., Saxena, G., Mungrue, I. N., Lusis, A. J. & Shalev, A. Thioredoxin-interacting protein: a critical link between glucose toxicity and beta-cell apoptosis. *Diabetes* **57,** 938–944 (2008).

© 2010 Macmillan Publishers Limited. All rights reserved.

23. Hui, S. T. *et al.* Txnip balances metabolic and growth signaling via PTEN disulfide reduction. *Proc. Natl Acad. Sci. USA* **105,** 3921–3926 (2008).
24. Zhang, C. Y. *et al.* Uncoupling protein-2 negatively regulates insulin secretion and is a major link between obesity, beta cell dysfunction, and type 2 diabetes. *Cell* **105,** 745–755 (2001).
25. Rosen, E. D. & Spiegelman, B. M. Adipocytes as regulators of energy balance and glucose homeostasis. *Nature* **444,** 847–853 (2006).
26. Sreekumar, R., Halvatsiotis, P., Schimke, J. C. & Nair, K. S. Gene expression profile in skeletal muscle of type 2 diabetes and the effect of insulin treatment. *Diabetes* **51,** 1913–1920 (2002).
27. Tamemoto, H. *et al.* Insulin resistance and growth retardation in mice lacking insulin receptor substrate-1. *Nature* **372,** 182–186 (1994).
28. Muoio, D. M. & Newgard, C. B. Mechanisms of disease: molecular and metabolic mechanisms of insulin resistance and beta-cell failure in type 2 diabetes. *Nat. Rev. Mol. Cell Biol.* **9,** 193–205 (2008).
29. Hackenbrock, C. R. Ultrastructural bases for metabolically linked mechanical activity in mitochondria. I. Reversible ultrastructural changes with change in metabolic steady state in isolated liver mitochondria. *J. Cell Biol.* **30,** 269–297 (1966).
30. Bonnard, C. *et al.* Mitochondrial dysfunction results from oxidative stress in the skeletal muscle of diet-induced insulin-resistant mice. *J. Clin. Invest.* **118,** 789–800 (2008).
31. Meglasson, M. D. & Matschinsky, F. M. Pancreatic islet glucose metabolism and regulation of insulin secretion. *Diabetes Metab. Rev.* **2,** 163–214 (1986).
32. MacDonald, M. J. Synergistic potent insulin release by combinations of weak secretagogues in pancreatic islets and INS-1 cells. *J. Biol. Chem.* **282,** 6043–6052 (2007).
33. Oberkofler, H., Klein, K., Felder, T. K., Krempler, F. & Patsch, W. Role of peroxisome proliferator-activated receptor-gamma coactivator-1alpha in the transcriptional regulation of the human uncoupling protein 2 gene in INS-1E cells. *Endocrinology* **147,** 966–976 (2006).
34. Medvedev, A. V. *et al.* Regulation of the uncoupling protein-2 gene in INS-1 beta-cells by oleic acid. *J. Biol. Chem.* **277,** 42639–42644 (2002).
35. Fan, M. *et al.* Suppression of mitochondrial respiration through recruitment of p160 myb binding protein to PGC-1alpha: modulation by p38 MAPK. *Genes Dev.* **18,** 278–289 (2004).
36. Ahsan, M. K., Nakamura, H., Masutani, H. & Yodoi, J. Thioredoxin and thioredoxin-binding protein-2 in cancer and metabolic syndrome. *Free Radic. Biol. Med.* **43,** 861–868 (2007).
37. Yoshihara, E., Chen, Z., Matsuo, Y., Masutani, H. & Yodoi, J. Thiol redox transitions by thioredoxin and thioredoxin-binding protein-2 in cell signaling. *Methods Enzymol.* **474,** 67–82 (2010).
38. Stoltzman, C. A. *et al.* Glucose sensing by MondoA:Mlx complexes: a role for hexokinases and direct regulation of thioredoxin-interacting protein expression. *Proc. Natl Acad. Sci. USA* **105,** 6912–6917 (2008).
39. Peterson, C. W., Stoltzman, C. A., Sighinolfi, M. P., Han, K. S. & Ayer, D. E. Glucose controls nuclear accumulation, promoter binding, and transcriptional activity of the MondoA-Mlx heterodimer. *Mol. Cell Biol.* **30,** 2887–2895 (2010).
40. Kaadige, M. R., Looper, R. E., Kamalanaadhan, S. & Ayer, D. E. Glutamine-dependent anapleurosis dictates glucose uptake and cell growth by regulating MondoA transcriptional activity. *Proc. Natl Acad. Sci. USA* **106,** 14878–14883 (2009).
41. Chen, J. L. *et al.* Lactic Acidosis Triggers Starvation Response with Paradoxical Induction of TXNIP through MondoA. *PLoS Genet.* **6,** e1001093 (2010).
42. Chutkow, W. A. *et al.* Deletion of the alpha-arrestin protein Txnip in mice promotes adiposity and adipogenesis while preserving insulin sensitivity. *Diabetes* **59,** 1424–1434 (2010).
43. Sesti, G. *et al.* Defects of the insulin receptor substrate (IRS) system in human metabolic disorders. *FASEB J.* **15,** 2099–2111 (2001).
44. Ferre, P. The biology of peroxisome proliferator-activated receptors: relationship with lipid metabolism and insulin sensitivity. *Diabetes* **53** (Suppl 1), S43–50 (2004).
45. Shaked, M. *et al.* Insulin counteracts glucotoxic effects by suppressing thioredoxin-interacting protein production in INS-1E beta cells and in Psammomys obesus pancreatic islets. *Diabetologia* **52,** 636–644 (2009).
46. Masson, E. *et al.* High beta-cell mass prevents streptozotocin-induced diabetes in thioredoxin-interacting protein-deficient mice. *Am. J. Physiol. Endocrinol. Metab.* **296,** E1251–1261 (2009).
47. Lin, C. H., MacGurn, J. A., Chu, T., Stefan, C. J. & Emr, S. D. Arrestin-related ubiquitin-ligase adaptors regulate endocytosis and protein turnover at the cell surface. *Cell* **135,** 714–725 (2008).
48. Hirasawa, T., Ohara, T. & Makino, S. Genetic typing of the mouse ob mutation by PCR and restriction enzyme analysis. *Exp. Anim.* **46,** 75–78 (1997).
49. Sutton, R., Peters, M., McShane, P., Gray, D. W. & Morris, P. J. Isolation of rat pancreatic islets by ductal injection of collagenase. *Transplantation* **42,** 689–691 (1986).
50. Fujimoto, S. *et al.* The novel insulinotropic mechanism of pimobendan: Direct enhancement of the exocytotic process of insulin secretory granules by increased Ca2+ sensitivity in beta-cells. *Endocrinology* **139,** 1133–1140 (1998).

Acknowledgments

We thank Dr Akira Kakizuka for kindly providing PGC-1α vector and helpful discussion. We also thank Dr Shunsuke Ishii for kindly providing Mybbp1a vector, Tamagawa Seiki Co. Ltd for providing tosyl-activated magnetic beads, Ms Ryoko Otsuki, Suzuyo Furukawa for technical assistance, Drs Eri Mukai and Yuichi Nishi for technical support and Drs Masahiko Sugita and Fuyuki Ishikawa for discussion. This work was supported by a Grant-in-Aid for Scientific Research from the Ministry of Education, Culture, Sports, Science, and Technology of Japan. This work was also supported in part by the Program for the Promotion of Fundamental Studies in Health Sciences of the National Institute of Biomedical Innovation (NIBIO). E.Y. was supported by a Research Fellowship from the Japan Society for the Promotion of Science for Young Scientists.

Author contributions

E.Y. designed and performed the experiments and wrote the manuscript with the help of S.F., N.I., J.Y. and H.M. E.Y., S.F., N.I and H.M. analysed the data. K.O. performed mass spectrometry analysis. S.M. prepared protein-immobilized beads. J.Y. directed the project as the principal investigator. H.M. supervised the study. All authors discussed the results and commented on the manuscript.

Additional information

Supplementary Information accompanies this paper on http://www.nature.com/naturecommunications

Competing financial interests: The authors declare no competing financial interests.

Reprints and permission information is available online at http://npg.nature.com/reprintsandpermissions/

How to cite this article: Yoshihara, E. *et al.* Disruption of TBP-2 ameliorates insulin sensitivity and secretion without affecting obesity. *Nat. Commun.* 1:127 doi: 10.1038/ncomms1127 (2010).

License: This work is licensed under a Creative Commons Attribution-NonCommercial-Share Alike 3.0 Unported License. To view a copy of this license, visit http://creativecommons.org/licenses/by-nc-sa/3.0/

© 2010 Macmillan Publishers Limited. All rights reserved.

RESEARCH PAPER

Islets 2:4, 247-251; July/August 2010; © 2010 Landes Bioscience

FGF-21 enhances islet engraftment in mouse syngeneic islet transplantation model

Taeko Uonaga,[1] Kentaro Toyoda,[1] Teru Okitsu,[2] Xiaotong Zhuang,[1] Shunsuke Yamane,[1] Shinji Uemoto[3] and Nobuya Inagaki[1,4,*]

[1]Department of Diabetes and Clinical Nutrition; Graduate School of Medicine; Kyoto University; Sakyo-ku, Kyoto Japan; [2]Transplantation Unit; Kyoto University Hospital; Kyoto, Japan; [3]Department of Surgery; Division of Hepato-Pancreato-Biliary Surgery and Transplantation; Graduate School of Medicine; Kyoto University; Kyoto, Japan; [4]CREST of Japan Science and Technology (JST); Kyoto, Japan

Key words: fibroblast growth factor-21, diabetes mellitus, islet transplantation, β-cell load, insulin sensitivity, cytoprotection, apoptosis

Abbreviations: FGF-21, fibroblast growth factor-21; STZ, streptozotocin; FGFs, fibroblast growth factors; FGFRs, their corresponding receptors; s.c., subcutaneously; IPGTT, intraperitoneal glucose tolerance test; AUC, area under the curve; HE, hematoxylin-eosine; i.p., intraperitoneal injection; HBSS, hanks balanced salt solution; HEPES, 4-(2-hydroxyethyl)-1-piperazineethanesulfonic acid; RIA, radioimmunoassay

To clarify the effect of fibroblast growth factor-21 (FGF-21) on islet transplantation, a suboptimal number of islets were transplanted into streptozotocin (STZ)-induced diabetic mice with or without FGF-21 treatment. Three-day treatment with FGF-21 contributed to restoration of normoglycemia by suppressing islet graft loss. The FGF-21-treated mice showed lower glycemic levels despite similar insulin content in the graft than that in untreated mice on day 3, indicating that FGF-21 not only has a cytoprotective effect but also decreases β-cell load by increasing insulin sensitivity. These results suggest that FGF-21 may be useful as a treatment to improve islet engraftment rates in clinical islet transplantation.

Do not distribute

Introduction

Fibroblast growth factors (FGFs) and their corresponding receptors (FGFRs) are known to be involved in the processes of development, transformation and angiogenesis.[1-4] The human FGF family consists of 22 members divided into seven subfamilies based on phylogeny and sequence identity.[1,5] On the other hand, FGFRs are divided into five distinct subtypes, FGFR-1 to -5, among which FGFR-1 and FGFR-2 are required for normal β-cell function and pancreatic development, respectively.[6-9] A co-factor usually is required for FGFs to bind and activate FGFR. Human FGF-21, which is mainly produced in liver, is a 181-amino-acid polypeptide and shares 75% amino acid sequence identity with mouse FGF-21.[10] FGF-21 together with FGF-19 and FGF-23 comprise the FGF-19 subfamily,[11] which is unique in that all three members are metabolic hormones involved in the regulation of glucose, lipid, bile acid and phosphate metabolism. FGF-21, the co-factor of which is βKlotho,[12,13] was first reported as a factor that might improve insulin sensitivity by upregulating glucose uptake into adipose tissue.[14] Subsequent studies showed that FGF-21 has various beneficial effects on pancreatic islets, increasing insulin synthesis and suppressing cytokine-induced apoptosis in isolated rat pancreatic islets and increasing glucose-induced insulin secretion from islets isolated from diabetic rodents.[15] Furthermore, FGF-21 reduces both plasma glucose and insulin levels not only in rodent diabetes models such as db/db mice but also in diabetic rhesus monkeys.[14-16]

Clinical islet transplantation has been performed world-wide since the report by Shapiro demonstrated 100% insulin independence in seven patients treated with a steroid-free, sirolimus-based immunosuppressant protocol, known as the Edmonton protocol.[17] However, one of the problems of this protocol is that multiple donors are required for insulin independence, mainly because of graft-loss caused by various stressors immediately after transplantation.[18,19] It is therefore especially important to reduce β-cell loss during this critical period.[20]

Because FGF-21 has various beneficial effects on islets, we investigated its effects on islet engraftment using syngeneic islet transplantation in diabetic mice with or without its administration during the critical 3 days after islet transplantation.

Results

FGF-21 ameliorated hyperglycemia in STZ-induced diabetic mice transplanted with a suboptimal number of islets. Eighty freshly isolated islets, which is a suboptimal number of islets for ameliorating hyperglycemia when transplanted alone, were transplanted into the left sub-renal capsule of STZ-induced diabetic mice. Immediately after transplantation, FGF-21 administration was begun subcutaneously (s.c.) twice daily for 3 days

*Correspondence to: Nobuya Inagaki; Email: inagaki@metab.kuhp.kyoto-u.ac.jp
Submitted: 03/01/10; Revised: 05/11/10; Accepted: 05/13/10
Previously published online: www.landesbioscience.com/journals/islets/article/12402

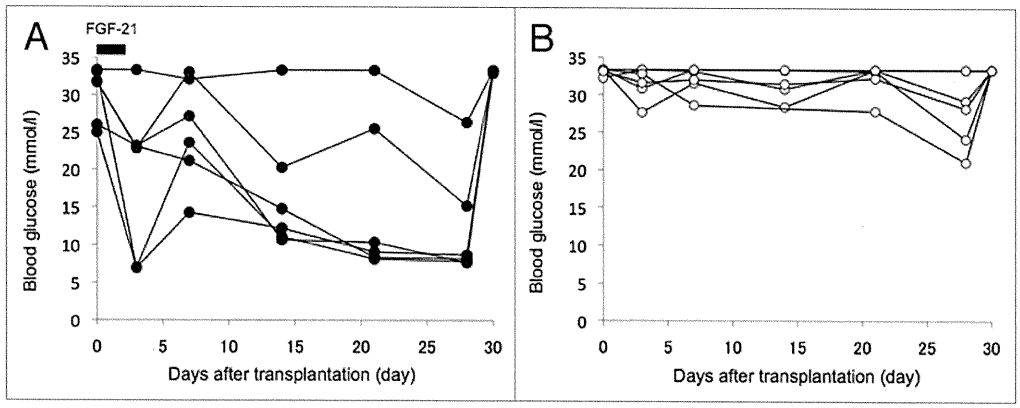

Figure 1. Non-fasting blood glucose levels in IT(+)/FGF(+) (closed circle, n = 6) (A) and IT(+)/FGF(-) mice (open circle, n = 5) (B).

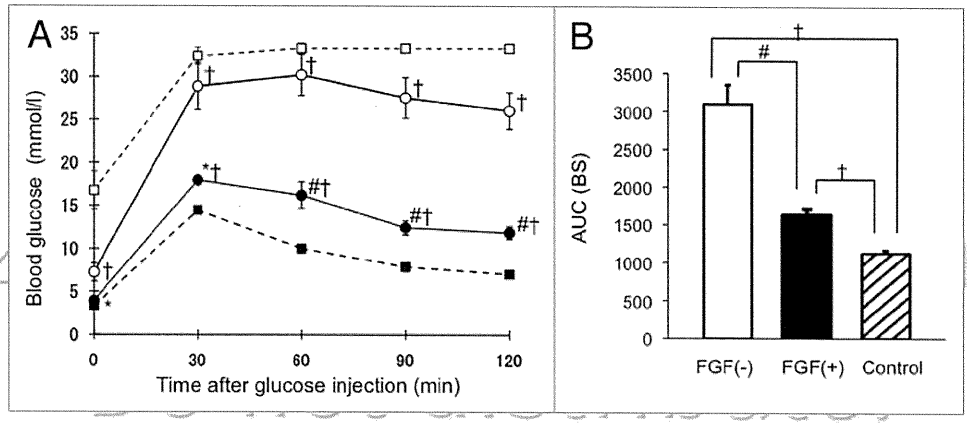

Figure 2. (A) Plasma glucose levels during i.p. glucose tolerance test (IPGTT) performed on day 30 in sham-operated wild-type C57BL/6 mice (control, dotted line, closed square, n = 5), in normoglycemic IT(+)/FGF(+) mice with non-fasting blood glucose level below 11.1 mM (closed circle, n = 4), in IT(+)/FGF(-) mice (open circle, n = 5), and in STZ-induced diabetic mice (dotted line, open square, n = 3). (B) AUC of blood glucose levels during IPGTT in wild-type control (lined bar), IT(+)/FGF(+) (black bar), and IT(+)/FGF(-) mice (white bar). *$p < 0.05$ vs. IT(+)/FGF(-). #$p < 0.01$ vs. IT(+)/FGF(-), †$p < 0.01$ vs. control.

(from day 0 through day 2). As control, 80 freshly isolated islets were similarly transplanted to STZ-induced diabetic mice but without FGF-21 treatment. As in our previous report, the criterion of normoglycemia was defined as a non-fasting blood glucose level below 11.1 mM (200 mg/dl) on at least two consecutive measurements on different day time points.[21]

After islet transplantation, 66.7% of the mice treated with FGF-21 (IT(+)/FGF(+) mice) became normoglycemic (**Fig. 1A**), while all of mice without FGF-21 treatment (IT(+)/FGF(-) mice) remained hyperglycemic (**Fig. 1B**). Mean blood glucose levels were significantly lower in IT(+)/FGF(+) mice than those in IT(+)/FGF(-) mice on day 3, and the difference continued thereafter (Day 0: 30.2 ± 1.5 vs. 33.1 ± 0.2 ($p = 0.11$), Day 3: 19.4 ± 4.3 vs. 31.6 ± 1.1 ($p < 0.05$), Day 7: 25.2 ± 2.9 vs. 32.0 ± 0.9 ($p = 0.07$), Day 14: 17.1 ± 3.6 vs. 31.4 ± 1.2 ($p < 0.05$), Day 21: 15.8 ± 4.4 vs. 32.2 ± 1.1 ($p < 0.01$), Day 28: 12.4 ± 3.0 vs. 28.2 ± 2.5 ($p < 0.01$) (mM)). The removal of the left kidney bearing the islet grafts resulted in hyperglycemia in all recipient mice (**Fig. 1**). Sham-operated STZ-induced diabetic mice with and without FGF-21 treatment showed persistent hyperglycemia (data not shown). These results indicate that FGF-21 improved glycemic control in islet-transplanted STZ-induced diabetic mice. Mean body weight on day 7 in IT(+)/FGF(+) mice was significantly lower than that in IT(+)/FGF(-) mice (20.3 g vs. 21.8 g, $p < 0.05$), but body weight on day 28 was similar in both of these mice (23.6 g vs. 23.1 g, $p = 0.35$).

FGF-21 treatment improved glucose tolerance 30 days after islet transplantation. To evaluate the degree of glucose tolerance, we performed intraperitoneal glucose tolerance test (IPGTT) on day 30 in hyperglycemic IT(+)/FGF(-) mice and normoglycemic IT(+)/FGF(+) mice (**Fig. 2A and B**). Blood glucose levels and area under the curve (AUC) during IPGTT in normoglycemic IT(+)/FGF(+) mice were significantly lower than those in hyperglycemic IT(+)/FGF(-) mice. However, both the blood glucose concentration and AUC in normoglycemic IT(+)/FGF(+) mice were not improved to the level observed in wild-type mice.

Islet grafts were more preserved in FGF-21-treated mice than those in untreated mice on day 30. To determine islet mass, we performed Hematoxylin-Eosine (HE) staining and insulin-immunostaining. Islet grafts in normoglycemic IT(+)/FGF(+) mice and those in hyperglycemic IT(+)/FGF(-) mice were detectable and comparable on day 3 (**Fig. 3A, B, E and**

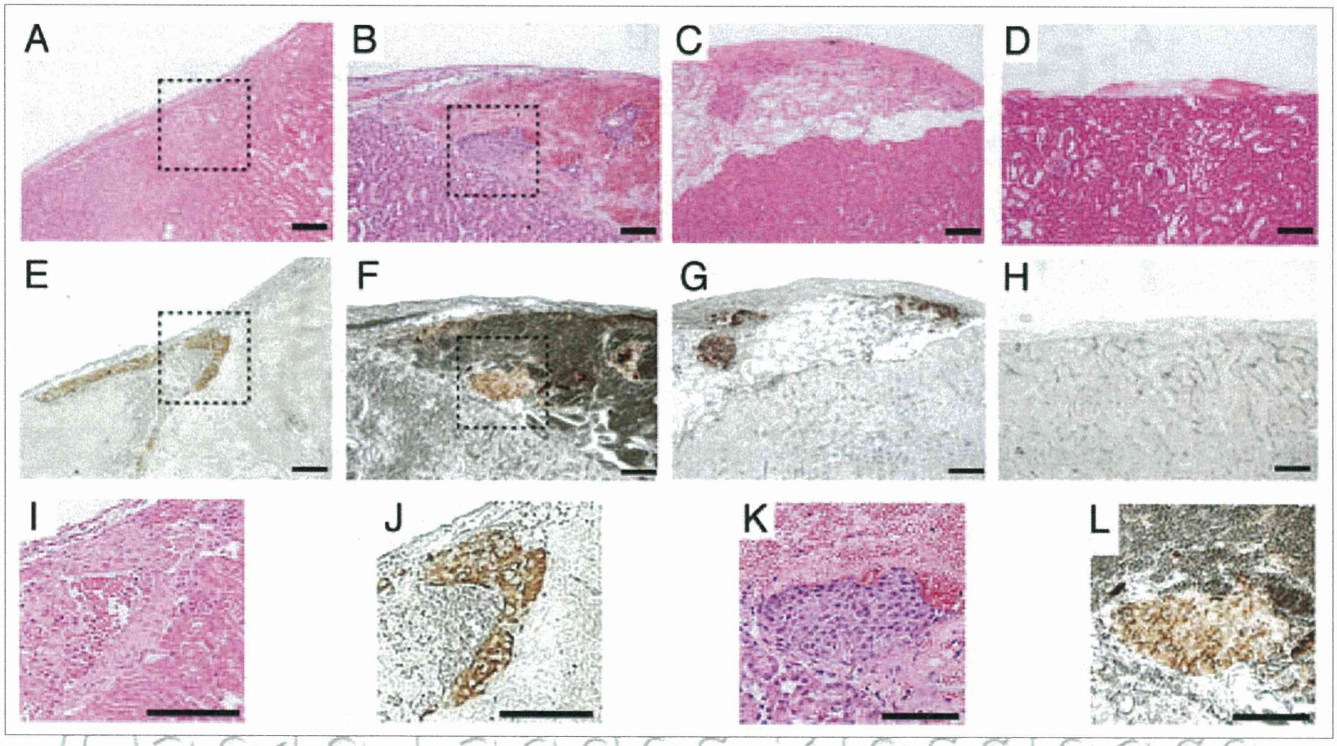

Figure 3. Immunohistochemical analysis of islet grafts from IT(+)/FGF(+) (A, C, E and G) and IT(+)/FGF(-) (B, D, F and H) mice. HE staining (x200) (A–D) and insulin-immunostaining (x200) (E–H) were performed. Ensquared areas in (A, B, E and F) are magnified in (I,K,J and L) respectively. Bar = 100 μm.

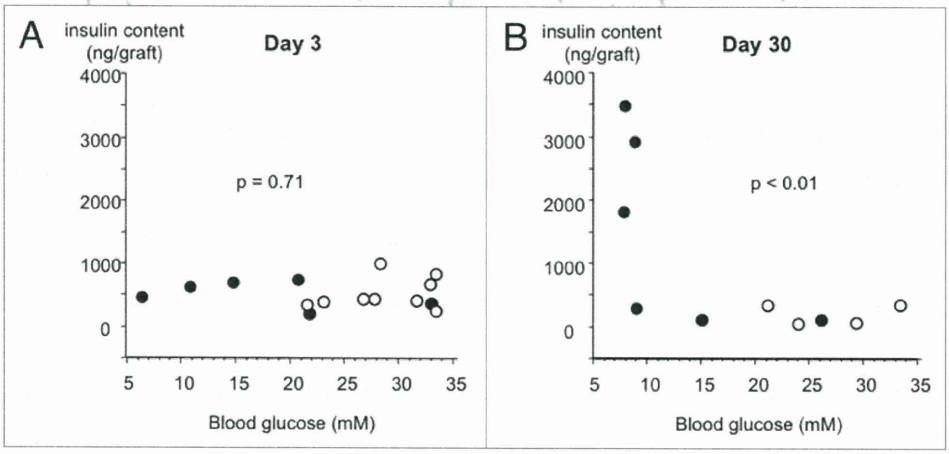

Figure 4. Insulin contents of islet grafts were measured in both IT(+)/FGF(+) (closed circle) and IT(+)/FGF(-) mice (open circle) on day 3 (A) and day 30 (B). Insulin contents of islet grafts were not correlated with the levels of blood glucose on day 3 ($p = 0.71$) (A), but were inversely correlated on day 30 ($p < 0.01$) (B).

F). Insulin content on day 3 in both mice was similar (**Fig. 4A**). However, on day 30, islet grafts in normoglycemic IT(+)/FGF(+) mice were more readily detectable (**Fig. 3C and G**), while those in IT(+)/FGF(-) mice were barely detectable (**Fig. 3D and H**). Consistently with this immunohistochemical finding, insulin content on day 30 in normoglycemic IT(+)/FGF(+) mice was significantly greater than that in untreated mice [2117.8 vs. 199.5 (ng/graft), $p < 0.05$] (**Fig. 4B**). We then analyzed the relationship between insulin content in the grafts and the non-fasting blood glucose level in all of the mice in both groups. Spearman rank correlation assessment showed that insulin content was inversely correlated with the non-fasting blood glucose level on day 30 ($p < 0.05$) (**Fig. 4B**), while no correlation was observed on day 3 ($p = 0.71$) (**Fig. 4A**).

Discussion

Here we demonstrate that FGF-21 promotes engraftment of islet transplants. Only 3-day treatment with FGF-21 resulted in more insulin content in the islet grafts on day 30 compared to that in untreated mice. As previously reported, insulin content is correlated not only with islet mass but also with the function of pancreatic β-cells.[22] Indeed, our data on day 30 show that the better the blood glucose level, the more insulin content in the islet grafts (**Fig. 4B**). Because the first several days after transplantation are known to be the most critical period for engraftment of islet transplants, 3-day treatment of FGF-21 was most likely to be responsible for the suppression of islet graft loss.

Regarding the mechanism of action, FGF-21 has been reported to improve insulin sensitivity in adipose tissue and in liver by upregulating glucose uptake and by inhibition of glucose production, respectively,[14,23] and has been shown acute glucose-lowering action even by a single injection.[24] In this study, the mean blood glucose level in normoglycemic IT(+)/FGF(+) mice was already significantly decreased compared to that in IT(+)/FGF(-) mice (15.0 ± 4.7 vs. 31.6 ± 1.1 (mM), $p < 0.01$) on day 3 (**Fig. 1**). Unfortunately, insulin levels during IPGTT were too low for comparison even by using a highly sensitive insulin assay kit. However, the decrease in blood glucose levels despite the similar insulin content (**Fig. 4B**) suggests that FGF-21 treatment increased insulin sensitivity, which might well decrease the β-cell load and rescue β-cells from apoptosis, as has previously been reported.[25-27] On the other hand, as FGF-21 treatment has been found to have a direct cytoprotective effect on pancreatic β-cells,[15] FGF-21 might well similarly affect the graft in our transplantation model. We attempted to examine this immunohistologically, but it was not possible to find statistical difference because only 80 islets were transplanted in our experiment.

Our results also reveal lower body weight in FGF-21-treated mice than that in untreated mice on day 3. A noteworthy advantage of FGF-21 use is that it does not elicit adverse effects such as hypoglycemia and weight gain,[15] which often result from insulin use. Many agents have been reported to be beneficial for islet transplantation,[27-29] but unlike FGF-21, only a few are conducive to a broad spectrum of beneficial effects such as increased β-cell survival, insulin secretion and insulin synthesis, as well as indirectly reducing β-cell load via increased insulin sensitivity. Furthermore, FGF-21 is free of proliferative and tumorgenic effects,[14,15,30] which are major problems with most growth factors.

Because the half-life of FGF-21 is about 1 h when subcutaneously injected in mice,[16,24] we administered FGF-21 twice a day. Only 3-day administration resulted in better glycemic control, suggesting that more frequent or continuous administration of FGF-21 for a longer period might achieve even better glycemic control without body weight gain or hypoglycemia. For more effective usage in a clinical setting, a controlled-release type of FGF-21 might be developed.

In conclusion, clinical use of FGF-21 has the potential to improve engraftment results in islet transplantation, although further studies, especially in human, must be performed to clarify its therapeutic potential.

Materials and Methods

Animal care. All experiments were approved by the Kyoto University Animal Care Committee.

Animals. Male C57BL/6JJcl mice (CREA, Japan) aged 9–13 weeks were used as donors and those aged 7–9 weeks were used as recipients. Recipient animals were rendered diabetic by a single intraperitoneal injection (i.p.) of streptozotocin (STZ) (Sigma-Aldrich, USA), 120 mg/kg body weight, freshly dissolved in 100 mM citrate buffer (pH 4.2). Mice with blood glucose concentration greater than 20 mM for 2 days were used as recipients. Blood glucose concentrations were determined by glucose meter (Glucocard, Arkley, Japan).

Islet isolation, islet transplantation and FGF-21 treatment. Under anesthesia, 2 ml of Hanks balanced salt solution (HBSS) containing 1 mg collagenase was injected into the common bile duct of the donor mouse. The distended pancreas was removed and incubated at 37°C for 21 min. Islets were purified by Ficoll-density centrifugation and 80 freshly isolated islets were transplanted into the left sub-renal capsule of the anesthetized recipient mouse. Human FGF-21 (BioVendor Laboratory Medicine, Ins. Czech Republic) was administered to the mice (1.67 mg/kg body weight/day) twice daily for three days.

Glucose tolerance test. On day 30, the mice were fasted for 16 h, blood samples were collected at 0, 30, 60, 90 and 120 min after glucose injection (1.0 g/kg body weight, i.p.), and blood glucose levels were measured.

Insulin content and immunohistochemistry. The renal capsule of the kidney containing the islet graft was removed on day 3 and day 30 for measurement of insulin content and immunohistochemical analysis, respectively. Renal capsules were frozen in 4 mM of 4-(2-hydroxyethyl)-1-piperazineethanesulfonic acid (HEPES), then thawed and homogenized by ultrasonic waves and insulin levels were measured by radioimmunoassay (RIA). Kidneys were fixed overnight in 4% paraformaldehyde and transferred into 70% ethanol before processing through paraffin. Rabbit anti-insulin antibody (sc-9168, 1:100, Santa Cruz Biotechnology Inc., Santa Cruz, USA) and HRP-Labeled anti-Rabbit antibody (Dako Cytomation EnVision + System, Denmark) were used to detect insulin as primary and secondary antibody, respectively.

Statistical analyses. All data are presented as mean ± SE. Statistical analyses were performed by unpaired t-test and the Spearman rank correlation was used to assess correlation between the data. p value of less than 0.05 was considered significant.

Acknowledgements

This work was supported by a Research Grant on Nanotechnical Medicine from the Ministry of Health, Labour and Welfare of Japan, and by Scientific Research Grants from the Ministry of Education, Culture, Sports, Science and Technology of Japan, and also by Kyoto University Global COE Program "Center for Frontier Medicine."

References

1. Ornitz DM, Itoh N. Fibroblast growth factors. Genome Biol 2001; 2:3005.
2. Eswarakumar VP, Lax I, Schlessinger J. Cellular signaling by fibroblast growth factor receptors. Cytokine Growth Factor Rev 2005; 16:139-49.
3. Grose R, Dickson C. Fibroblast growth factor signaling in tumorigenesis. Cytokine Growth Factor Rev 2005; 16:179-86.
4. Presta M, Dell'Era P, Mitola S, Moroni E, Ronca R, Rusnati M. Fibroblast growth factor/fibroblast growth factor receptor system in angiogenesis. Cytokine Growth Factor Rev 2005; 16:159-78.
5. Itoh N, Ornitz DM. Evolution of the Fgf and Fgfr gene families. Trends Genet 2004; 20:563-9.
6. Hart AW, Baeza N, Apelqvist A, Edlund H. Attenuation of FGF signalling in mouse betacells leads to diabetes. Nature 2000; 408:864-8.
7. Revest JM, Spencer-Dene B, Kerr K, De Moerlooze L, Rosewell I, Dickson C. Fibroblast growth factor receptor 2-IIIb acts upstream of Shh and Fgf4 and is required for limb bud maintenance but not for the induction of Fgf8, Fgf10, Msx1 or Bmp4. Dev Biol 2001; 231:47-62.
8. Celli G, LaRochelle WJ, Mackem S, Sharp R, Merlino G. Soluble dominant-negative receptor uncovers essential roles for fibroblast growth factors in multi-organ induction and patterning. EMBO J 1998; 17:1642-55.
9. Elghazi L, Cras-Meneur C, Czernichow P, Scharfmann R. Role for FGFR2IIIb-mediated signals in controlling pancreatic endocrine progenitor cell proliferation. Proc Natl Acad Sci USA 2002; 99:3884-9.
10. Nishimura T, Nakatake Y, Konishi M, Itoh N. Identification of a novel FGF, FGF-21, preferentially expressed in the liver. Biochim Biophys Acta 2000; 1492:203-6.
11. Itoh N. The Fgf families in humans, mice and zebrafish: their evolutional processes and roles in development, metabolism and disease. Biol Pharm Bull 2007; 30:1819-25.
12. Kurosu H, Choi M, Ogawa Y, Dickson AS, Goetz R, Eliseenkova AV, et al. Tissue-specific expression of betaKlotho and fibroblast growth factor (FGF) receptor isoforms determines metabolic activity of FGF19 and FGF21. J Biol Chem 2007; 282:26687-95.
13. Ogawa Y, Kurosu H, Yamamoto M, Nandi A, Rosenblatt KP, Goetz R, et al. BetaKlotho is required for metabolic activity of fibroblast growth factor 21. Proc Natl Acad Sci USA 2007; 104:7432-7.
14. Kharitonenkov A, Shiyanova TL, Koester A, Ford AM, Micanovic R, Galbreath EJ, et al. FGF-21 as a novel metabolic regulator. J Clin Invest 2005; 115:1627-35.
15. Wente W, Efanov AM, Brenner M, Kharitonenkov A, Koster A, Sandusky GE, et al. Fibroblast growth factor-21 improves pancreatic beta-cell function and survival by activation of extracellular signal-regulated kinase 1/2 and Akt signaling pathways. Diabetes 2006; 55:2470-8.
16. Kharitonenkov A, Wroblewski VJ, Koester A, Chen YF, Clutinger CK, Tigno XT, et al. The metabolic state of diabetic monkeys is regulated by fibroblast growth factor-21. Endocrinology 2007; 148:774-81.
17. Shapiro AM, Lakey JR, Ryan EA, Korbutt GS, Toth E, Warnock GL, et al. Islet transplantation in seven patients with type 1 diabetes mellitus using a glucocorticoid-free immunosuppressive regimen. N Engl J Med 2000; 343:230-8.
18. Eich T, Eriksson O, Lundgren T. Visualization of early engraftment in clinical islet transplantation by positron-emission tomography. N Engl J Med 2007; 356:2754-5.
19. Barshes NR, Wyllie S, Goss JA. Inflammation-mediated dysfunction and apoptosis in pancreatic islet transplantation: implications for intrahepatic grafts. J Leukoc Biol 2005; 77:587-97.
20. Ryan EA, Paty BW, Senior PA, Bigam D, Alfadhli E, Kneteman NM, et al. Five-year follow-up after clinical islet transplantation. Diabetes 2005; 54:2060-9.
21. Yonekawa Y, Okitsu T, Wake K, Iwanaga Y, Noguchi H, Nagata H, et al. A new mouse model for intraportal islet transplantation with limited hepatic lobe as a graft site. Transplantation 2006; 82:712-5.
22. McCulloch DK, Koerker DJ, Kahn SE, Bonner-Weir S, Palmer JP. Correlations of in vivo beta-cell function tests with beta-cell mass and pancreatic insulin content in streptozocinadministered baboons. Diabetes 1991; 40:673-9.
23. Xu J, Lloid DJ, Hale C, Stanislaus S, Chen M, Sivits G, et al. Fibroblast growth factor 21 reverses hepatic steatosis, increases energy expenditure, and improves insulin sensitivity in diet-induced obese mice. Diabetes 2009; 58:250-9.
24. Xu J, Stanislaus S, Chinookoswong N, Lau YY, Hager T, Patel J, et al. Acute glucose-lowering and insulin-sensitizing action of FGF21 in insulin resistant mouse models—Association with liver and adipose tissue effects. Am J Physiol Endocrinol Metab 2009; 297: 1105-14.
25. Biarnes M, Montolio M, Nacher V, Raurell M, Soler J, Montanya E. Beta-cell death and mass in syngeneically transplanted islets exposed to short- and long-term hyperglycemia. Diabetes 2002; 51:66-72.
26. Merino JF, Nacher V, Raurell M, Aranda O, Soler J, Montanya E. Improved outcome of islet transplantation in insulin-treated diabetic mice: effects on beta-cell mass and function. Diabetologia 1997; 40:1004-10.
27. King A, Lock J, Xu G, Bonner-Weir S, Weir GC. Islet transplantation outcomes in mice are better with fresh islets and exendin-4 treatment. Diabetologia 2005; 48:2074-9.
28. Toyoda K, Okitsu T, Yamane S, Uonaga T, Liu X, Harada N, et al. GLP-1 receptor signaling protects pancreatic beta cells in intraportal islet transplant by inhibiting apoptosis. Biochem Biophys Res Commun 2008; 367:793-8.
29. Contreras JL, Eckstein C, Smyth CA, Bilbao G, Vilatoba M, Ringland SE, et al. Activated protein C preserves functional islet mass after intraportal transplantation: a novel link between endothelial cell activation, thrombosis, inflammation and islet cell death. Diabetes 2004; 53:2804-14.
30. Huang X, Yu C, Jin C, Yang C, Xie R, Cao D, et al. Forced expression of hepatocyte-specific fibroblast growth factor 21 delays initiation of chemically induced hepatocarcinogenesis. Mol Carcinog 2006; 45:934-42.

Landes Bioscience
Do not distribute

ORIGINAL ARTICLE

Exendin-4 Suppresses Src Activation and Reactive Oxygen Species Production in Diabetic Goto-Kakizaki Rat Islets in an Epac-Dependent Manner

Eri Mukai,[1,2] Shimpei Fujimoto,[1] Hiroki Sato,[1] Chitose Oneyama,[3] Rieko Kominato,[1] Yuichi Sato,[1] Mayumi Sasaki,[1] Yuichi Nishi,[1] Masato Okada,[3] and Nobuya Inagaki[1,4]

OBJECTIVE—Reactive oxygen species (ROS) is one of most important factors in impaired metabolism secretion coupling in pancreatic β-cells. We recently reported that elevated ROS production and impaired ATP production at high glucose in diabetic Goto-Kakizaki (GK) rat islets are effectively ameliorated by Src inhibition, suggesting that Src activity is upregulated. In the present study, we investigated whether the glucagon-like peptide-1 signal regulates Src activity and ameliorates endogenous ROS production and ATP production in GK islets using exendin-4.

RESEARCH DESIGN AND METHODS—Isolated islets from GK and control Wistar rats were used for immunoblotting analyses and measurements of ROS production and ATP content. Src activity was examined by immunoprecipitation of islet lysates followed by immunoblotting. ROS production was measured with a fluorescent probe using dispersed islet cells.

RESULTS—Exendin-4 significantly decreased phosphorylation of Src Tyr416, which indicates Src activation, in GK islets under 16.7 mmol/l glucose exposure. Glucose-induced ROS production (16.7 mmol/l) in GK islet cells was significantly decreased by coexposure of exendin-4 as well as PP2, a Src inhibitor. The Src kinase–negative mutant expression in GK islets significantly decreased ROS production induced by high glucose. Exendin-4, as well as PP2, significantly increased impaired ATP elevation by high glucose in GK islets. The decrease in ROS production by exendin-4 was not affected by H-89, a PKA inhibitor, and an Epac-specific cAMP analog (8CPT-2Me-cAMP) significantly decreased Src Tyr416 phosphorylation and ROS production.

CONCLUSIONS—Exendin-4 decreases endogenous ROS production and increases ATP production in diabetic GK rat islets through suppression of Src activation, dependently on Epac. ***Diabetes* 60:218–226, 2011**

From the [1]Department of Diabetes and Clinical Nutrition, Graduate School of Medicine, Kyoto, University, Kyoto, Japan; the [2]Japan Association for the Advancement of Medical Equipment, Tokyo, Japan, the [3]Department of Oncogene Research, Research Institute for Microbial Diseases, Osaka University, Osaka, Japan; and the [4]Core Research for Evolutional Science and Technology of Japan Science and Technology Cooperation, Kyoto, Japan.

Corresponding author: Shimpei Fujimoto, fujimoto@metab.kuhp.kyoto-u.ac.jp.

Received 6 January 2010 and accepted 12 October 2010. Published ahead of print at http://diabetes.diabetesjournals.org on 26 October 2010. DOI: 10.2337/db10-0021.

© 2011 by the American Diabetes Association. Readers may use this article as long as the work is properly cited, the use is educational and not for profit, and the work is not altered. See http://creativecommons.org/licenses/by-nc-nd/3.0/ for details.

The costs of publication of this article were defrayed in part by the payment of page charges. This article must therefore be hereby marked "advertisement" in accordance with 18 U.S.C. Section 1734 solely to indicate this fact.

In pancreatic β-cells, glucose metabolism regulates exocytosis of insulin granules through metabolism secretion coupling, in which glucose-induced ATP production in mitochondria plays an essential role (1). Impairment of mitochondrial ATP production causes reduced glucose-induced insulin secretion.

Reactive oxygen species (ROS) is one of the most important factors that impair metabolism secretion coupling in β-cells. Exposure to exogenous hydrogen peroxide (H_2O_2), the most abundant ROS, reduces glucose-induced insulin secretion by impairing mitochondrial metabolism in β-cells (2,3). However, little is known of the role of endogenous ROS in impaired glucose-induced insulin secretion from β-cells. Some studies (4,5) have shown that endogenous ROS is produced in mitochondria by exposure to high glucose. In Zucker diabetic fatty rats, the superoxide content of islets at basal glucose levels is higher than that in Zucker lean control rats (4). Furthermore, we recently reported that high glucose–induced ROS production in islet cells is elevated in diabetic Goto-Kakizaki (GK) rats compared with control Wistar rats (6). Thus, endogenous ROS production is elevated in β-cells under diabetic pathophysiological conditions.

Although the mechanism of endogenous ROS production in β-cells in the diabetic state remains largely unknown, we have reported that Src (c-Src) plays an important role in the signal transduction that produces ROS (6). Src is a nonreceptor tyrosine kinase that is associated with the cell membrane and plays important roles in various signal transductions, and its activity is regulated by intramolecular interactions that depend on tyrosine phosphorylation (7,8). Phosphorylation of Tyr527 (Tyr529 in humans), which is located near the C terminus of Src, is brought about by COOH terminal Src kinase (Csk), a negative regulator of Src (9), and holds the kinase in the inactive form. Dephosphorylation of Tyr527 followed by disruption of the intramolecular interaction allows phosphorylation of Tyr416 (Tyr418 in humans) at the kinase domain, resulting in Src activation. In our previous report (6), PP2, a selective Src inhibitor, decreased high-glucose–induced ROS production in GK islet cells, in contrast to the lack of any effect of the agent in Wistar islet cells, suggesting that Src may be activated in the diabetic condition and cause elevation of ROS production in the presence of high glucose.

Glucagon-like peptide (GLP)-1 is one of the incretin peptides released from the intestine in response to nutrient ingestion that augments glucose-induced insulin secretion from β-cells (10,11). GLP-1 binding to the GLP-1 receptor, a member of the G protein–coupled receptor

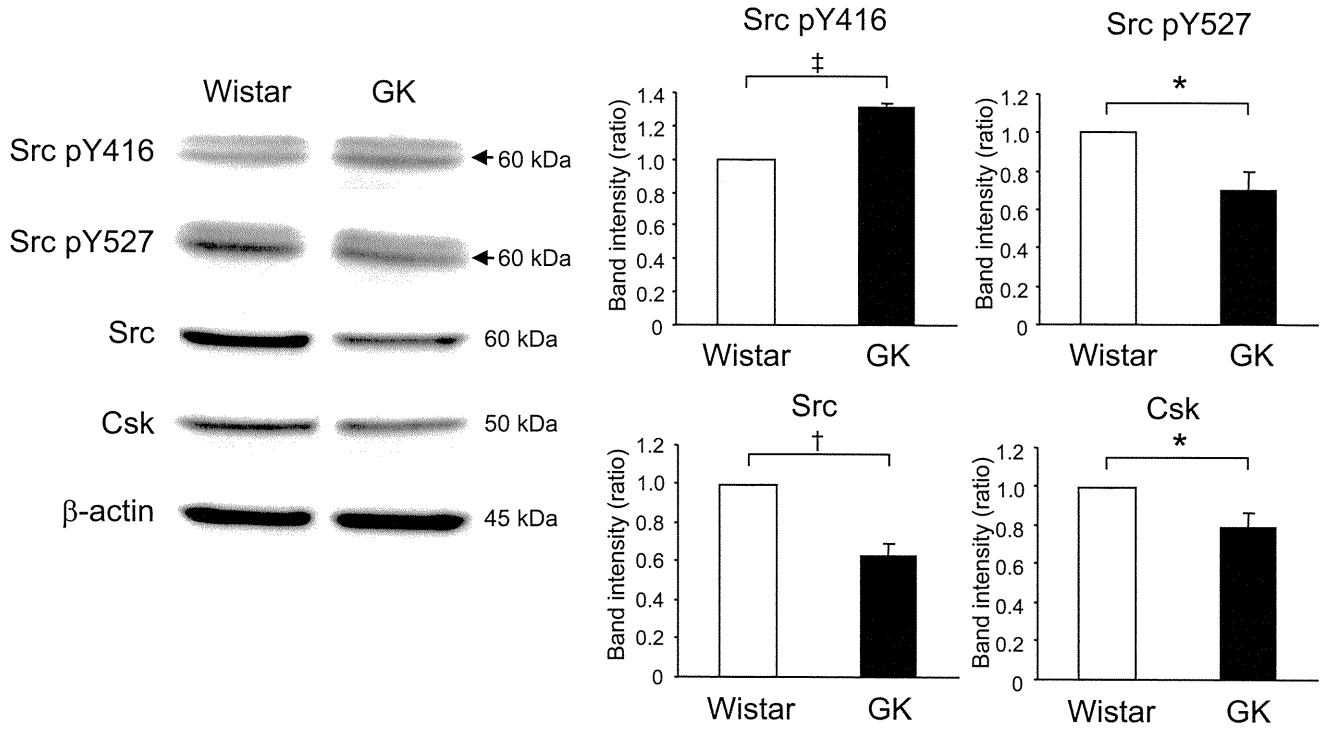

FIG. 1. Comparison of expression of Src between fresh Wistar and GK islets. Fresh islets were lysated and subjected to immunoblot analyses. Blots (50 μg of protein) were probed with anti–phospho-Src (Tyr^{416}), anti–phospho-Src (Tyr^{527}), anti-Src, or anti-Csk. The same blots were stripped and reprobed with anti–β-actin, respectively. Intensities of the bands were quantified with densitometric imager. The bar graphs are expressed relative to Wistar islet value corrected by β-actin level (means ± SE). *$P < 0.05$; †$P < 0.01$; ‡$P < 0.001$. Representative blot panels of three to five independent experiments are shown.

(GPCR) superfamily, induces activation of adenylyl cyclase and elevation of intracellular cAMP levels, which elicits protein kinase A (PKA)-dependent signal transduction. Recently, Epac (also known as cAMP-GEF [guanine nucleotide exchange factor]) has been shown to be a novel cAMP sensor in the PKA-independent pathway (12,13). In β-cells, one member of the Epac family, Epac2, has an important role in insulin secretion, especially in regulation of exocytosis of insulin granules (14,15). Previous studies have shown that GLP-1 also has beneficial long-term effects on diabetic β-cells, including induction of β-cell proliferation (16,17), enhanced resistance to apoptosis (17,18), and amelioration of endoplasmic reticulum stress (19). Furthermore, increased ROS in diabetic *db/db* mouse islets is decreased by treatment with an inhibitor of dipeptidyl peptidase IV that delays the degradation of GLP-1 (20).

In the present study, we investigated whether the GLP-1 signal directly ameliorates endogenous ROS production in diabetic GK islets using exendin-4, a GLP-1 receptor agonist. In particular, we focused on clarifying regulation of Src activity by GLP-1 signaling. We describe here both a novel effect and a mechanism of GLP-1 signaling that acutely decreases ROS production by high glucose through suppression of Src activation PKA independently and Epac dependently.

RESEARCH DESIGN AND METHODS

Male Wistar and GK rats were obtained from Shimizu (Kyoto, Japan). All experiments were carried out with rats that were aged ~7–8 weeks. Nonfasting blood glucose levels were ~160–240 mg/dl in the GK rats and ~70–120 mg/dl in the Wistar rats used in the experiments. The animals were maintained and used in accordance with the guidelines of the animal care committee of Kyoto University.

Islet preparation. Pancreatic islets were isolated from Wistar and GK rats by the collagenase digestion technique (6). Isolated islets were washed with Krebs Ringer bicarbonate buffer (KRBB) (in mmol/l: 129.4 NaCl, 5.2 KCl, 2.7 $CaCl_2$, 1.3 KH_2PO_4, 1.3 $MgSO_4$, and 24.8 $NaHCO_3$ [equilibrated with 5% CO_2/95% O_2, pH 7.4]) containing 2.8 mmol/l glucose and cultured for ~20 h in RPMI-1640 medium containing 5.5 mmol/l glucose and 10% FCS. Cultured islets were preincubated for 30 min at 37°C in KRBB supplemented with 0.2% BSA and 10 mmol/l HEPES (KRBB medium) containing 2.8 mmol/l glucose and incubated for the indicated times at 37°C in KRBB medium containing 16.7 mmol/l glucose with or without test materials.

Retroviral-mediated gene transfer. Production of retroviral vectors with pCX4 was performed as previously described (21). Src kinase–negative mutant (K295M) was subcloned into pCX4pur (22). Gene transfer experiments of islets were carried out by an in vivo gene transduction method (23). Briefly, after rats were anesthetized and subjected to laparotomy, the hepatic artery with the portal vein and the splenic artery were ligated. The upper side of the celiac artery that branches from the abdominal aorta was clamped, and 100 μl of retroviral vector suspension was injected into the lower side of the clamped point of the artery. The pancreatic islets were then isolated and cultured for 48 h before the experiment. Gene expression using green fluorescent protein–expressing vector was effective in the inside of the islets, as previously reported (23).

Immunoprecipitation and immunoblotting. Fresh or incubated islets were lysed in ice-cold lysis buffer (10 mmol/l Tris [pH 7.2], 100 mmol/l NaCl, 1 mmol/l EDTA, 1% Nonidet P-40, and 0.5% sodium deoxycholate) containing protease inhibitor cocktail (Complete; Roche, Mannheim, Germany), phosphatase inhibitor cocktail (Calbiochem, Darmstadt, Germany), and 5 mmol/l sodium pyrophosphate. For determination of Src activation, lysates were centrifuged at 560,000*g* for 10 min at 4°C, and the supernatant (~2 mg of protein content/2,500 islets) was mixed with 4 μg mouse monoclonal anti-Src antibody (clone GD11; Upstate, Billerica, MA) and 30 μl washed protein G Sepharose (GE Healthcare, Uppsala, Sweden) followed by gentle rotation for 4 h at 4°C. Immunoprecipitates or islet lysates (50 μg) were subjected to immunoblotting as previously described (23). Primary antibodies used were rabbit anti–phospho-Src (Tyr416) and anti–phospho-Src (Tyr527) from Biosource (Camarillo, CA); rabbit anti-Src, anti-Csk, anti-Epac2, extracellular signal–regulated kinase (ERK) 1/2, and mouse anti–phospho-ERK1/2 (Thr202/Tyr204) from Santa Cruz Biotechnology (Santa Cruz, CA); rabbit anti-Rap1 from Upstate; rabbit anti–phospho-Akt (Ser473) and anti-Akt from Cell

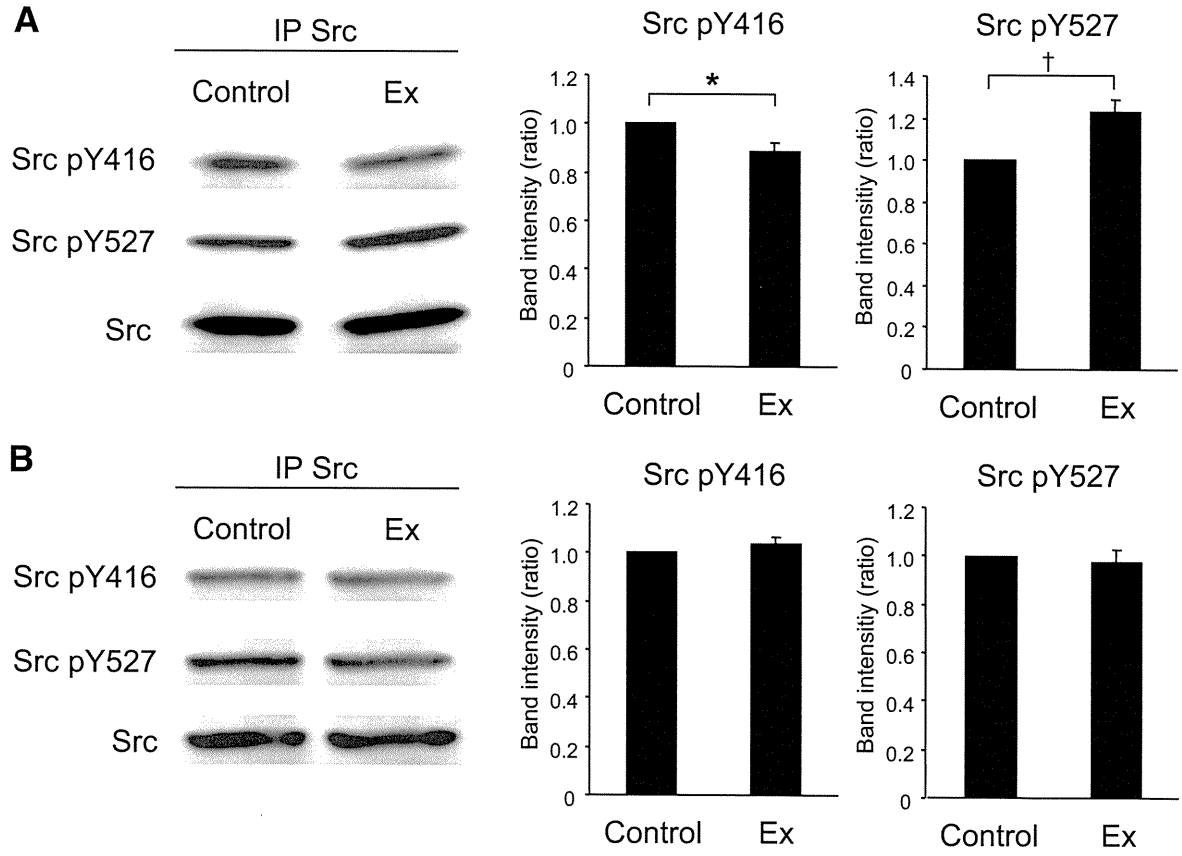

FIG. 2. Exendin-4 suppresses Src activity at high glucose in GK islets. Effects of exendin-4 on Src activity at high glucose in GK (*A*) and Wistar (*B*) islets. After preincubation in the presence of 2.8 mmol/l glucose for 30 min, islets were incubated in the presence of 16.7 mmol/l glucose with or without 100 nmol/l exendin-4 for 10 min. Islet lysates (~2 mg of protein) were immunoprecipitated with anti-Src antibody and subjected to immunoblot analyses. Blots were probed with anti–phospho-Src (Tyr^{416}), anti–phospho-Src (Tyr^{527}), or anti-Src by stripping and reprobing of the same blots. Intensities of the bands were quantified with densitometric imager. The bar graphs are expressed relative to control value corrected by Src level (means ± SE). *$P < 0.05$; †$P < 0.01$. Representative blot panels of four (*A*) or three (*B*) independent experiments are shown.

Signaling (Danvers, MA); and mouse anti–β-actin from Sigma (St. Louis, MO). Secondary antibodies used were horseradish peroxidase–conjugated anti-rabbit and mouse antibody (GE Healthcare). Band intensities were quantified with Multi Gauge software (Fujifilm, Tokyo, Japan).

Measurement of ROS production. ROS production in islet cells was measured by 2′,7′-dichlorofluorescein fluorescence (6). Briefly, cultured islets were dispersed using 0.05% trypsin/0.53 mmol/l EDTA (Invitrogen, Carlsbad, CA) and PBS. Dispersed islet cells were preincubated in KRBB medium containing 2.8 mmol/l glucose and 10 μmol/l 5-(and 6-) chloromethyl-2′,7′-dichlorodihydrofluorescein diacetate (CM-H_2DCFDA; Invitrogen) for 20 min at 37°C. After a 60-min incubation in 400 μl KRBB medium containing 16.7 mmol/l glucose with or without test materials, fluorescence was measured using a spectrofluorophotometer (RF-5300PC; Shimadzu, Kyoto, Japan), with excitation wavelength at 505 nm and emission wavelength at 540 nm. Fluorescence was corrected by subtracting parallel blanks and represented by fold increases of the value at time zero.

Measurement of ATP content. ATP content in islets was determined by luminometry as previously described (6). Briefly, after preincubation, groups of 10 islets were batch incubated for 30 min in KRBB medium containing 2.8 or 16.7 mmol/l glucose with or without test materials. Incubation was stopped immediately by addition of $HClO_4$ and sonication in ice-cold water for 10 min. They were then centrifuged, and a fraction of the supernatant was mixed with HEPES and Na_2CO_3. The ATP content in the supernatant of islet lysates was measured using ENLITEN luciferase/luciferin reagent (Promega, Madison, WI) with a luminometer (GloMax 20/20n; Promega).

Materials. Exendin-4 and forskolin were purchased from Sigma. PP2 was purchased from Tocris (Ellisville, MO). PP3, H-89, myristoylated PKA inhibitor amide14–22 (PKI), LY294002, wortmannin, PD98059, and AG1478 were purchased from Calbiochem. Dibutyryl cAMP was purchased from Daiichisankyo (Tokyo, Japan). 8-(4-chlorophenylthio)-2′-*O*-methyl-cAMP (8CPT-2Me-cAMP) was purchased from Biolog Life Science (Bremen, Germany).

Statistical analysis. Data are expressed as means ± SE. Statistical significance of difference was evaluated by the unpaired Student *t* test. $P < 0.05$ was considered significant.

RESULTS

Comparison of expression of Src between Wistar and GK islets. To examine whether the expression levels of Src in GK islets differ from those in Wistar islets, immunoblotting using fresh islets was performed. As shown in Fig. 1*A*, the level of Src pY416, which indicates activation of Src, in GK islets was significantly higher than that in Wistar islets. The levels of Src pY527, total Src, and Csk in GK islets were significantly lower than those in Wistar islets. The levels of other Src family kinases (SFKs) were similar in Wistar and GK islets, whereas the expression of Fgr was very low and that of Fyn was undetectable (supplementary Fig. 1 in the online appendix, available at http://diabetes.diabetesjournals.org/cgi/content/full/db10-0021/DC1). Results of immunoblotting using islets cultured for 20 h in the presence of 5.5 mmol/l glucose (supplementary Fig. 2) were similar to those shown in Fig. 1*A*.

Exendin-4 suppresses Src activity in GK islets. To investigate whether exendin-4 regulates Src activity, phosphorylation of Src was examined by immunoprecipitation and immunoblotting. As shown in Fig. 2*A*, Src pY416 was

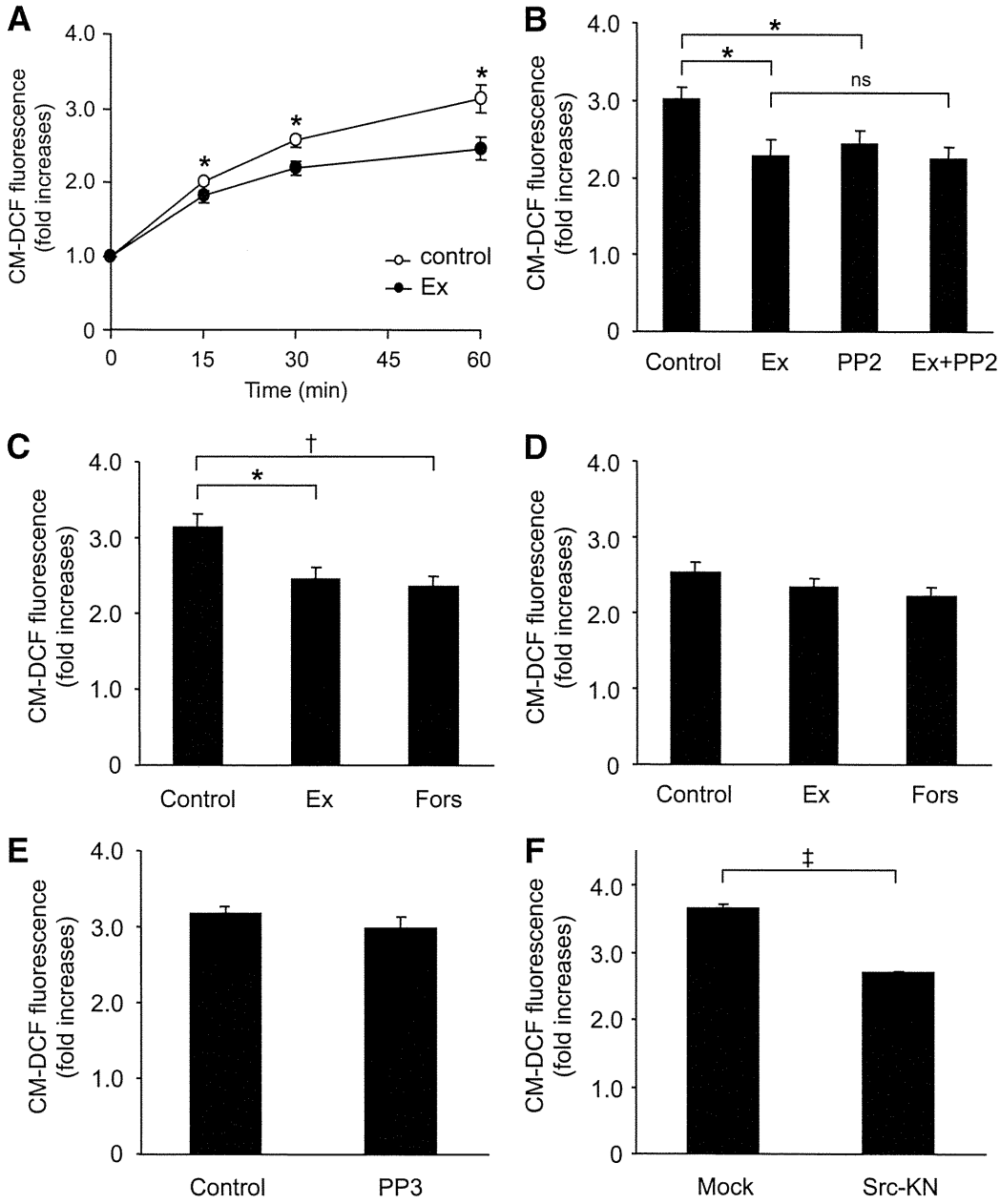

FIG. 3. Exendin-4 decreases ROS production at high glucose in GK islet cells. *A*: Time course of high-glucose–induced ROS production with or without 100 nmol/l exendin-4 in GK islet cells. After preincubation in the presence of 2.8 mmol/l glucose and 10 μmol/l CM-H_2DCFDA for 20 min, dispersed islet cells were incubated in the presence of 16.7 mmol/l glucose with (●) or without (○) 100 nmol/l exedin-4 for 60 min. Fluorescence is represented as fold increases against the value at time zero. Data are expressed as means ± SE (n = 5–7). *P < 0.05 vs. control. *B*: Effects of exendin-4 and PP2 on high-glucose–induced ROS production at 60 min in GK islet cells. Data are expressed as means ± SE (n = 4–6). *P < 0.05. *C*: Effects of exendin-4 and forskolin on high-glucose–induced ROS production at 60 min in GK islet cells. Data are expressed as means ± SE (n = 5–6). *P < 0.05; †P < 0.01. *D*: Effects of exendin-4 and forskolin on high-glucose–induced ROS production at 60 min in Wistar islet cells. Data are expressed as means ± SE (n = 3–4). *E*: Effects of PP3 on high-glucose–induced ROS production at 60 min in GK islet cells. Data are expressed as means ± SE (n = 3). *F*: Effect of Src-KN on high-glucose–induced ROS production at 60 min in GK islet cells. Retroviral (empty vector and Src-KN vector)-mediated gene transfer to islets was carried out by in vivo gene transduction method, as described in RESEARCH DESIGN AND METHODS. Data are expressed as means ± SE (n = 3). ‡P < 0.001.

significantly decreased by 100 nmol/l exendin-4 in the presence of 16.7 mmol/l glucose in GK islets. Exendin-4 also significantly increased Src pY527 in GK islets in the same condition. On the other hand, exendin-4 did not affect Src pY416 or pY527 at high glucose in Wistar islets (Fig. 2*B*). Both Src pY416 and pY527 were not altered by change in glucose concentration in GK or Wistar islets (supplementary Fig. 3).

Exendin-4 decreases ROS production in GK islet cells. We then investigated whether exendin-4 ameliorates endogenous ROS production at high glucose in GK islet cells. A total of 16.7 mmol/l glucose exposure induced ROS production in GK islet cells (Fig. 3*A*). Coexposure of exendin-4 significantly decreased ROS production in the presence of 16.7 mmol/l glucose at 15, 30, and 60 min. A total of 10 μmol/l PP2, a Src inhibitor, significantly de-

creased high-glucose–induced ROS production (Fig. 3*B*), but PP3, the inactive PP2 analog, did not affect it (Fig. 3*E*). Exendin-4 did not further decrease ROS production in the presence of PP2 (Fig. 3*B*), suggesting that the effect of exendin-4 is via the Src signal. The decrease in high-glucose–induced ROS production also was observed in the presence of 10 μmol/l forskolin, an adenylyl cyclase activator (Fig. 3*C*). High-glucose–induced ROS production in Wistar islet cells was lower than that in GK islet cells and was not changed by addition of exendin-4 or forskolin (Fig. 3*D*). To confirm that Src is actually involved in ROS production, we measured ROS production in GK islets expressing a kinase-negative form of Src (Src-KN) by retroviral vector. ROS production in Src-KN–expressing islets was significantly lower than that in control (Fig. 3*F*), demonstrating that Src regulates ROS production in GK islets.

Exendin-4 increases ATP content in GK islets. In Wistar islets, 16.7 mmol/l glucose-exposure significantly increased ATP content compared with that in the presence of 2.8 mmol/l glucose, as shown in Fig. 4*B*. Exendin-4, PP2, or exendin-4 plus PP2 did not affect the ATP content in the presence of 16.7 mmol/l glucose in Wistar islets. The ATP content in GK islets exposed to 16.7 mmol/l glucose was not increased compared with that in the presence of 2.8 mmol/l glucose (Fig. 4*A*). Exendin-4 as well as PP2 significantly increased the ATP content in the presence of 16.7 mmol/l glucose. Further increase of ATP content by combined exendin-4 and PP2 was not observed.

The effects of exendin-4 are dependent on Epac. We then investigated whether the decrease in ROS production by exendin-4 is dependent on PKA. As shown in Fig. 5*A*, decreased ROS production by exendin-4 or forskolin was not affected by 10 μmol/l H-89 or PKI, a PKA inhibitor, indicating that the effect is PKA independent. Not only dibutyryl cAMP, a general cAMP analog, but also 8CPT-2Me-cAMP, an Epac-specific cAMP analog, decreased ROS production (Fig. 5*C*). Epac possesses guanine nucleotide exchange factor activity toward Rap1, a member of the Ras superfamily of small GTPases. Epac2 and Rap1 proteins were expressed similarly in both Wistar and GK islets (Fig. 5*B*). To determine involvement of Epac in Src activation, Src phosphorylation was examined. Src pY416 was significantly decreased by 8CPT-2Me-cAMP (Fig. 5*D*).

A downstream pathway of Src is PI3K/Akt signaling. Src signalings toward downstream proteins are complex, but one of the typical pathways is phosphatidylinositol 3 kinase (PI3K)/Akt signaling (8). We therefore examined the involvement of PI3K/Akt signaling on ROS production. A total of 50 μmol/l LY294002 and 0.5 μmol/l wortmannin, both of which are PI3K inhibitors, significantly decreased ROS production in GK islets (Fig. 6*A*). Exendin-4 and PP2 both significantly decreased phosphorylation of Akt in GK islets (Fig. 6*B*) but not in Wistar islets (Fig. 6*C*). Considering these findings together, PI3K/Akt signaling that produces ROS is located downstream of Src activation. We also examined the involvement of mitogen-activated protein kinase signaling, another downstream pathway of Src. A total of 50 μmol/l PD98059, a MAPK-ERK kinase inhibitor, did not affect ROS production in GK islets (Fig. 6*D*), and neither exendin-4 nor PP2 affected phosphorylation of ERK (Fig. 6*E*). Several GPCR agonists have been shown to induce transactivation of epidermal growth factor receptor (EGFR) (24,25) by a mechanism involving Src (25–27) and frequently subsequent PI3K/Akt signaling (25,28). Therefore, involvement of EGFR transactivation on regulation of ROS production was examined. A total of 0.5 μmol/l AG1478, an EGFR kinase inhibitor, significantly decreased ROS production (Fig. 6*F*).

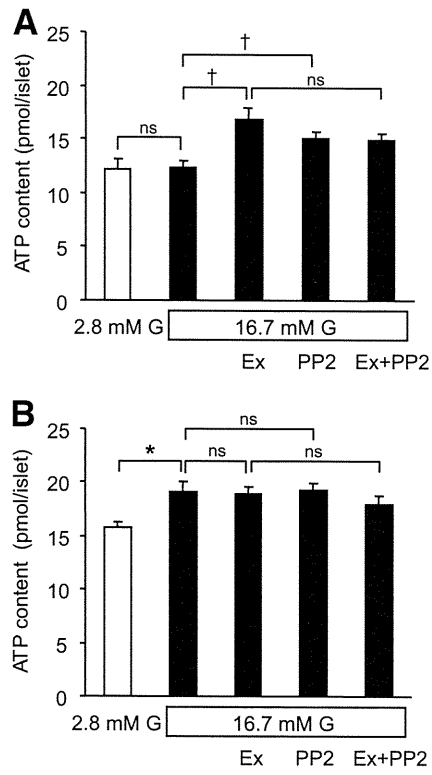

FIG. 4. Exendin-4 increases ATP content at high glucose in GK islets. Effects of exendin-4 and PP2 on ATP content in the presence of high glucose for 30 min in GK (*A*) and Wistar (*B*) islets. After preincubation in the presence of 2.8 mmol/l glucose for 30 min, islets were incubated in the presence of 2.8 or 16.7 mmol/l glucose with or without 100 nmol/l exendin-4, 10 μmol/l PP2, or both for 30 min. Data are expressed as means ± SE (n = 7–8). *P < 0.05; †P < 0.01.

DISCUSSION

We previously reported that endogenous ROS production by high glucose in diabetic GK islets is elevated compared with that in control Wistar islets and is effectively ameliorated by Src inhibition, suggesting that Src may be activated in GK islets (6). In the present study, we first investigated whether Src activity is altered in GK islets. Immunoblotting analysis revealed that the level of Src pY416, which indicates the level of Src activation, is higher in GK islets than that in Wistar islets, despite lower levels of total Src, Src pY527, and Csk. The lower level of total Src seems to be a consequence of Src activation. Targeted degradation of active forms of Src is brought about by ubiquitination (29). The protooncogene c-Cbl, recently found to be an E3 ubiquitin ligase, mediates ubiquitination of activated Src (30). These reports suggest that increased degradation of activated Src may result in a lower level of total Src in GK islets. In addition, a lower level of Csk might cause a lower activity of the kinase in GK islets. However, Src activity is not directly regulated through phosphorylation of Tyr527 by Csk (8), and a subtle decrease in Csk activity is not believed to contribute to regulation of Src activity because of the excess amount of expression of Csk. This is supported by the findings that heterozygous disruption of ubiquitously expressed Csk

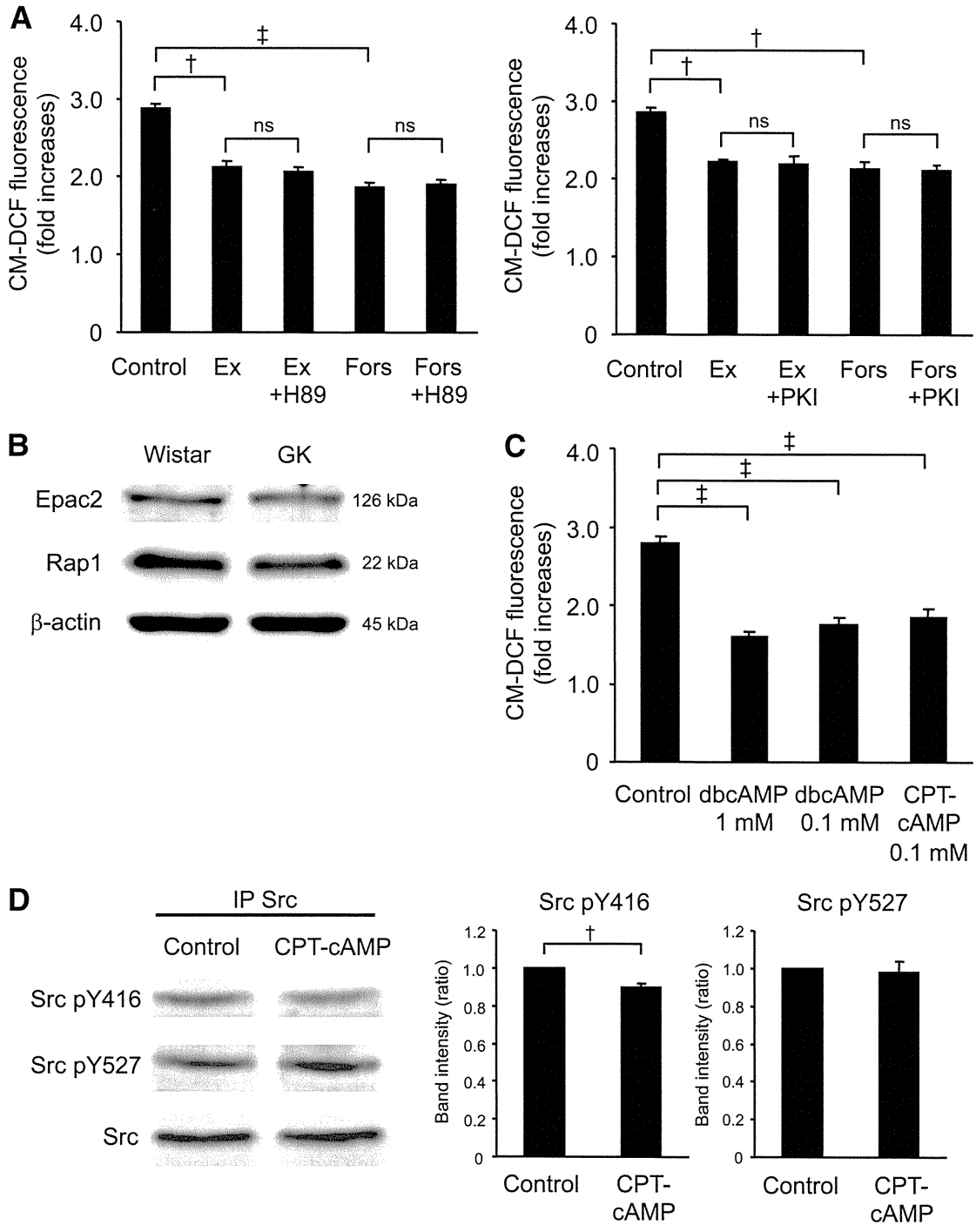

FIG. 5. The effects of exendin-4 are dependent not on PKA but on Epac. *A*: Effects of H-89 or PKI on the decrease in high-glucose–induced ROS production by exendin-4 or forskolin at 60 min in GK islet cells. After preincubation in the presence of 2.8 mmol/l glucose and 10 μmol/l CM-H_2DCFDA for 20 min, dispersed islet cells were incubated in the presence of 16.7 mmol/l glucose with or without 100 nmol/l exendin-4 or 10 μmol/l forskolin with or without 10 μmol/l H-89 or 10 μmol/l PKI for 60 min. Fluorescence is represented as fold increases against the value at time zero. Data are expressed as means ± SE (n = 3). †P < 0.01; ‡P < 0.001. *B*: Expression of Epac2 and Rap1 in Wistar and GK islets. Fresh islets were lysated and subjected to immunoblot analyses. Blots (50 μg of protein) were probed with anti-Epac2 or anti-Rap1. The same blots were stripped and reprobed with anti–β-actin, respectively. Representative blot panels of three independent experiments are shown. *C*: Effects of cAMP analogs on high-glucose–induced ROS production at 60 min in GK islet cells. Data are expressed as means ± SE (n = 3–4). ‡P < 0.001. *D*: Epac-specific cAMP analog suppresses Src activity at high glucose in GK islets. After preincubation in the presence of 2.8 mmol/l glucose for 30 min, islets were incubated in the presence of 16.7 mmol/l glucose with or without 0.1 mmol/l 8CPT-2Me-cAMP for 8 min. Islet lysates (~2 mg of protein) were immunoprecipitated with anti-Src antibody and subjected to immunoblot analyses. Blots were probed with anti–phospho-Src (Tyr^{416}), anti–phospho-Src (Tyr^{527}), or anti-Src by stripping and reprobing of the same blots. Intensities of the bands were quantified with densitometric imager. The bar graphs are expressed relative to control value corrected by Src level (means ± SE). †P < 0.01. Representative blot panels of four independent experiments are shown.